

# ITSC-16 Addendum

## Towards a better use of AMSU over land at ECMWF

***Blazej Krzeminski<sup>1)</sup>, Niels Bormann<sup>1)</sup>, Fatima Karbou<sup>2)</sup> and Peter Bauer<sup>1)</sup>***

*<sup>1)</sup> European Centre for Medium-range Weather Forecasts (ECMWF), Shinfield Park, Reading, RG1 9AX, United Kingdom*

*<sup>2)</sup> CNRM-GAME, Météo France, 42 avenue de Coriolis, 31057, Toulouse, France*

### Introduction

Assimilation of observed clear-sky brightness temperatures (BT) with variational methods requires calculation of their equivalent First Guess BTs. At ECMWF, they are calculated from 4DVar First Guess (FG) atmospheric profiles using the RTTOV radiative transfer (RT) code. In the case of surface sensitive channels, a good estimation of surface emission is needed for these RT calculations. Accurate microwave land emissivity models typically require input parameters describing surface characteristics, rarely available globally. As a compromise, simplified emissivity models are usually employed, resulting in the significant errors in the simulated BTs. Retrieving emissivities directly from the microwave window channel observations is currently being investigated at ECMWF as an alternative approach. Experiments have shown that using retrieved emissivities significantly reduces FG-departures over land for AMSU-A surface sensitive channels 1-5 and AMSU-B channel 2. This has a direct impact on the quality control of the other AMSU channels. Assimilating surface sensitive channels with the new emissivity scheme also seems to have positive impact on forecast skill. Other topics discussed here include changes to the bias correction and quality control procedures over land.

### Current use of AMSU-A and -B over land at ECMWF

Clear-sky AMSU-A/B and MHS radiances are assimilated operationally in the IFS 4DVar system. Over land AMSU-A channels 5-14 have influence on the analysed atmospheric state. Channel 4 is not assimilated due to its strong sensitivity to the surface emission. For the same reason, channel 5 is used only over orography not exceeding 500m and the limit for channel 6 is 1500m. For AMSU-B (and MHS), only channels 3 and 4 are assimilated, both over low orography only.

AMSU observations are bias corrected prior to their assimilation. In the IFS system, an adaptive variational bias correction scheme (VarBC) is implemented (Auligné et al., 2007).

Bias corrected AMSU-A observations are subject to quality control, partly to eliminate cloud and rain contaminated observations in the tropospheric channels 5-7. These quality checks are based on the differences between observations and their clear-sky equivalents simulated from the IFS first guess atmospheric profiles (FG-departures). Channels 5-7 are rejected if the channel 4 FG-departure exceeds +/- 0.7 K. Rain contaminated observations are detected explicitly using the difference between

23.8 GHz and 89 GHz observations (scattering index). Differences larger than 3 K indicates the presence of rain.

The quality control for the AMSU-B channels 3 and 4 over land is done by applying a +/- 5K threshold test to the channel 2 FG-departures.

AMSU-A land surface emissivities are estimated using an algorithm described in detail in Kelly (2000). The method uses window channels 1, 2 and 3 to identify the surface type. Different emissivity models are then applied for different surfaces. In practice, for non-polar regions, more than 99% of locations are identified as "dry/wet land including vegetation" (statistics for November 2006) and the emissivity is computed with the regression formula:

$$\varepsilon = -4.119 \cdot 10^{-2} - 9.0916 \cdot 10^{-3} \cdot BT_{23GHz} + 1.2172 \cdot 10^{-2} \cdot BT_{31GHz} + 4.8851 \cdot 10^{-4} \cdot BT_{50GHz} \quad (1)$$

The land surface emissivity model for AMSU-B is a simple lookup table, representing four possible surface types (table 1). The surface type at a given location is classified using the IFS information about the surface temperature, soil moisture and snow cover.

Table 1: AMSU-B emissivity lookup table

surface type	emissivity
moist land	0.95
light snow	0.95
dry land	0.92
deep snow	0.80

The accuracy of the surface emissivity estimation is important for the assimilation of the tropospheric channels as well as for the performance of the QC tests that utilize window channel FG-departures. The currently used algorithms do not take into account variations of the emissivity with the scan angle and frequency. Additionally the emissivities from the regression formula display unrealistic diurnal tendencies. An alternative approach in which the land emissivities are retrieved directly from the window channel observations is currently under evaluation at ECMWF.

### Dynamic emissivity retrievals

Brightness Temperature  $BT$  observed by the spaceborne instrument can be expressed as

$$BT_{obs} = \varepsilon T_s \Gamma + BT_{up} + \Gamma(1 - \varepsilon)BT_{down}$$

where  $T_s$  is the radiation emitted by the surface,  $\varepsilon$  is the surface emissivity,  $BT_{up}$  and  $BT_{down}$  are the atmospheric upwelling and down-welling radiances respectively and  $\Gamma$  is the atmospheric surface-to-space transmissivity. By rearranging the above equation, surface emissivity can be calculated:

$$\varepsilon = \frac{BT_{obs} - BT_{up} - BT_{down}\Gamma}{(T_s - BT_{down})\Gamma}$$

This is under the assumption of the specular reflection from the surface (Karbou, 2005) and non-scattering plane parallel atmosphere.

The method was implemented at Météo France within the ARPEGE 4DVar system and later ported to the IFS 4DVar (Prigent et al., 2005).  $BT_{up}$ ,  $BT_{down}$  and  $\Gamma$  are estimated with the RTTOV

radiative transfer code from the IFS First Guess forecast profiles. A selected window channel provides the observed BT.

The retrieved emissivity is then used to estimate surface emission for the assimilation of the other AMSU surface sensitive channels over land. In our experiments we tried AMSU-A channel 2 (31.4 GHz) which has the smallest atmospheric contribution from all AMSU-A channels, and channel 3 (50.3 GHz) which should provide emissivity retrievals more representative of the other sounding channels around 50 GHz. For AMSU-B, channel 1 (89 GHz) retrievals were investigated. Figure 1 shows an emissivity map obtained by averaging the emissivities retrieved from 50.3 GHz observations.

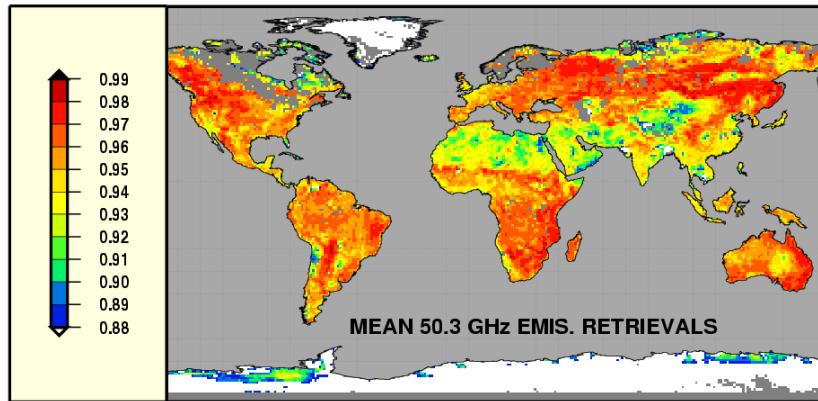


Fig.1: Emissivity retrievals averaged over 1 month (26 Sep 2006 - 26 Oct 2006). NOAA-16 AMSU-A channel 3 observations close to nadir were used for the retrievals.

### Comparison with FASTEM emissivities

Retrieved emissivities were compared against FASTEM2 (Deblonde, 2000) over sea for clear-sky conditions. AMSU-A emissivities generally show a good correlation. The retrieval scheme occasionally gives higher emissivities than FASTEM - possibly due to the residual cloud or rain warm signal in the observations over the radiatively cold ocean background. AMSU-B emissivities are less consistent - they are sensitive to the errors in the water vapour profiles of the first guess forecast.

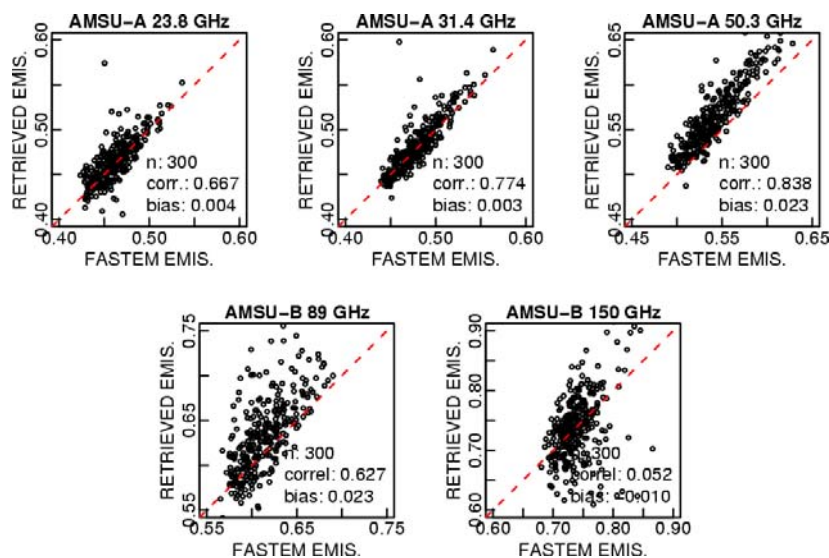


Fig.2: Comparison of FASTEM and retrieved ocean emissivities; A sample of NOAA-16 observations over sea after cloud/rain screening and collocated IFS first guess atmospheric

profiles was used for the retrievals; emissivities retrieved from AMSU-A channels 1,2,3 and AMSU-B channels 1,2 are shown. A random sample of cases spans 2 days.

### Changes in the bias correction

In the operational setup, biases in the FG-departures are corrected using the VarBC scheme. In the case of the AMSU instrument, this includes correction of the global mean bias followed by the removal of the scan angle dependent bias component. These corrections are applied globally, with no distinction between land and ocean areas. However, biases in the FG-departures of surface sensitive channels over land and water can have different characteristics as a result of using different emissivity models. As there is much more data available over ocean, it is expected to dominate the bias estimations. Indeed, operational bias correction removes bias over water (not shown) but significant residual biases can be observed over land for AMSU-A channel 4 (fig.3) and channel 5. It was therefore desirable to separate the bias correction over different areas.

It should be noted that using the retrieved emissivities already reduces the residual biases in the FG-departures over land (fig.3b,3c). Nevertheless a separate bias correction over land was tested and resulted in further reduction of the bias (fig.3d).

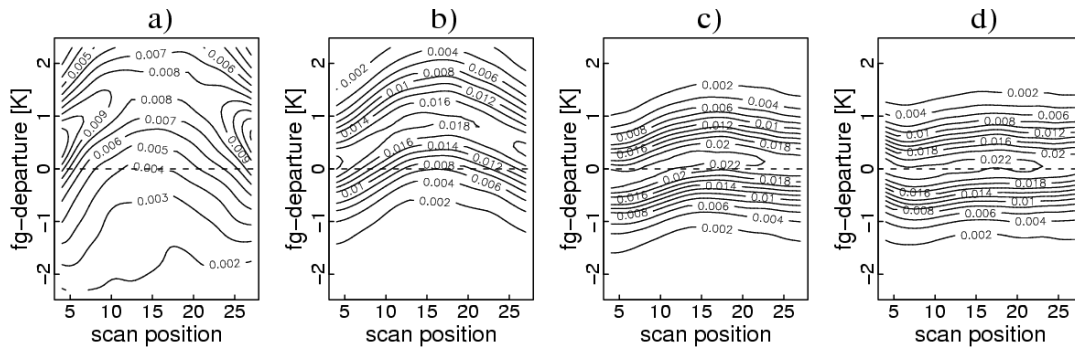


Fig. 3: Density distribution of the NOAA-16 AMSU-A channel 4 FG-departures for different scan positions. Data after the bias correction are shown. a) FG-departures over land with the operational emissivity scheme, b) FG-departures over land with 31.4 GHz retrieved emissivities, c) FG-departures over land calculated with 50.3 GHz retrieved emissivities, d) FG-departures over land calculated with 50.3 GHz emissivities and with separate bias correction applied.

### Changes in the quality control

Cloud and rain contaminated AMSU observations should be excluded from the assimilation if the emission and scattering from the cloud water and ice particles is not modeled in the radiative transfer calculations. As described earlier, observations are screened by comparing them with the equivalent clear-sky First Guess BTs (FG-departure threshold test). Such tests work reasonably well to identify cloudy observations over water - they will be significantly “warmer” over the radiatively cold ocean background than the clear-sky First Guess BTs. However, over land, the clear-sky surface emission is typically very similar to the cloud emission making this type of cloud detection problematic (Huang, 1992).

In an attempt to improve the quality of the used data, an additional simple QC test was applied experimentally over land. AMSU-A channel 5-7 and AMSU-B channel 3-5 were excluded from the assimilation if the vertically integrated First Guess cloud liquid water exceeded  $0.03 \text{ kg/m}^2$  within the

FOV. AMSU-A channel 4 FG-departure threshold test was retained as a safety net but relaxed from +/- 0.7 to +/- 1.2 K over land. AMSU-B FG-departure test remained unchanged.

Comparison of the QC performance with the METEOSAT images suggests improved cloud detection skill of the revised test (fig.4). The number of good quality data presented to the assimilation is significantly higher with the new emissivity and revised QC in use (fig.5)

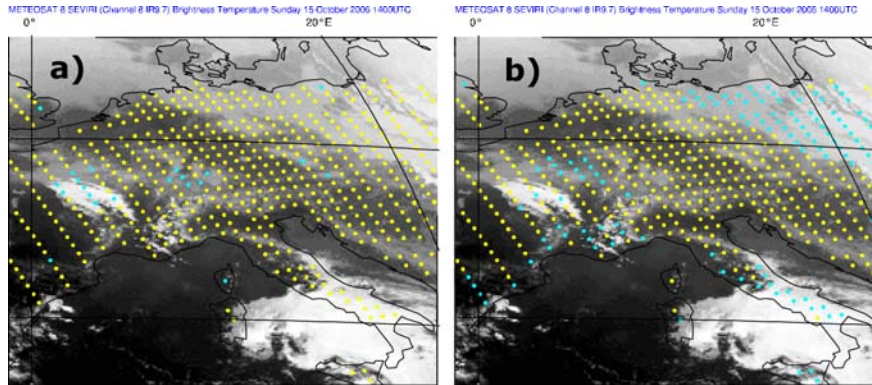


Fig.4: AMSU-A QC results validated against the METEOSAT-8 9.7 $\mu$ m images. Panel (a) shows the results of the old QC - some cloudy scenes are not detected by the +/- 0.7K channel 4 FG-departure test. The same scenes are correctly marked as cloudy (blue dots on the panel b) by the new First Guess liquid water content QC test. Emissivities retrieved from AMSU-A channel 3 observations were used in both cases.

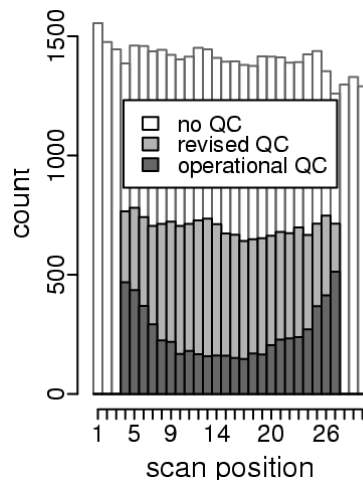


Fig.5: Number NOAA-16 AMSU-A of observations passing QC. The new emissivity scheme together with the revised quality control results in more observations passing the QC compared to the operational configuration. The strong residual scan bias in channel 4 FG-departures is responsible for large variations in the operational QC performance with the scan position. This effect is reduced with the revised QC and new emissivity scheme (emissivities were retrieved from 50.3 GHz observations).

### Impact on the RT calculations

The dynamic emissivity retrievals result in the First Guess estimations of the observed BTs that are more consistent with the observations for the surface sensitive channels. FG-departures for AMSU-A channels 1-5 and AMSU-B channel 2 are reduced compared to the operations (fig.6).

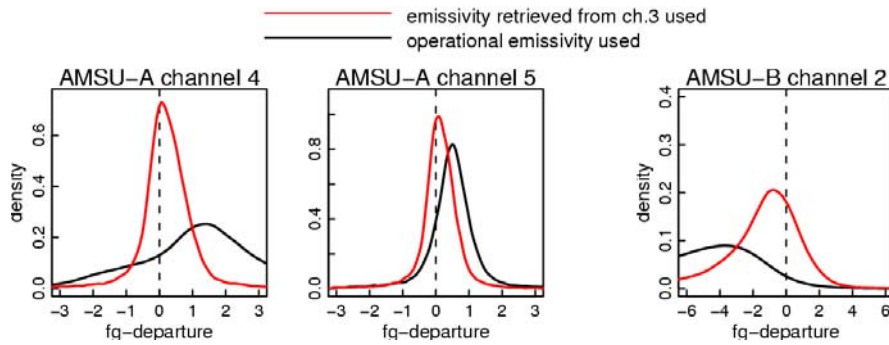


Fig.6: Normalized histograms of the FG-departures for NOAA-16 AMSU-A and -B surface sensitive channels for the operational and experimental emissivity scheme. AMSU-A channel 3 and AMSU-B channel 1 were used to retrieve emissivities.

One reason for the observed significant FG-departure variations are the diurnal tendencies in the operational land emissivity estimated with the regression formula (1). The day-night difference in the estimated emissivity is around 0.07, which translates to about 2K diurnal difference in the channel 4 FG-departures (fig.7). The new emissivity scheme removes these diurnal variations.

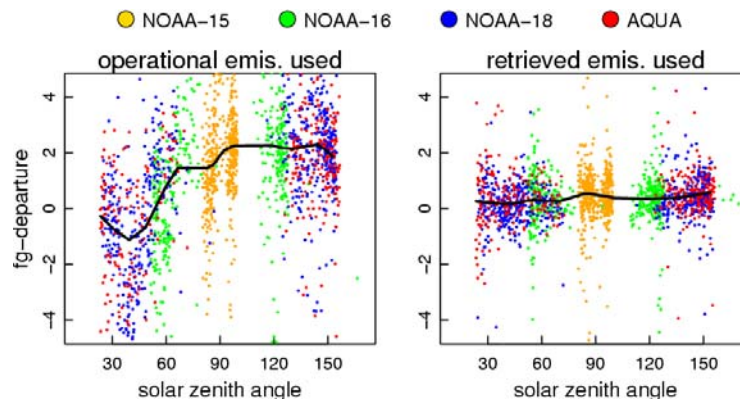


Fig.7: AMSU-A channel 4 FG-departures as a function of the solar zenith angle for the old and new emissivity scheme. Channel 3 was used on the second panel for the emissivity retrievals.

## Impact on the forecasts

To assess the impact of the new emissivity scheme on the ECMWF forecast accuracy, a series of forecasts spanning a 2 month period, 26 Aug 2006 - 26 Oct 2006, was run. AMSU-A observations were assimilated with the emissivities estimated from either channel 2 or 3 (31.4 or 50.3 GHz respectively). For AMSU-B, channel 1 (89 GHz) was used for the emissivity retrievals. Response of the forecast system to the changes in the bias correction and quality control was also tested. Overall, all changes combined together resulted in the improved forecasts. Using 50.3 GHz emissivities for AMSU-A assimilation improves forecasts both over the northern and southern hemisphere for the first 3-4 days of the forecast (fig.8).

With the 31.4 GHz emissivities, impact over the northern hemisphere was neutral (not shown).

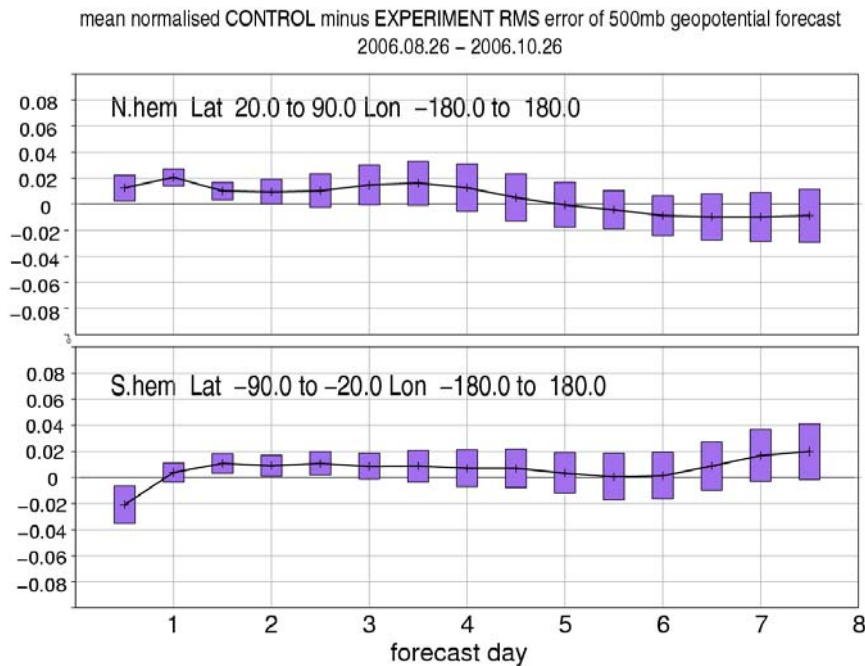


Fig.8: Normalized difference in 500mb geopotential RMS forecast error between the control and the experiment with revised emissivity, bias correction and QC schemes. Positive values mean smaller RMS errors in the experiment. A population of 62 forecasts was used to calculate the statistics (bars indicate 90% confidence level for the null-hypothesis that the RMS forecast errors of the two experiments were identical).

## Summary and future work

Emissivity retrievals are a promising approach for the land emissivity estimation and have the advantage of being relatively simple to implement in the NWP model. Using the retrievals in the RT calculations of the First Guess brightness temperatures over land resulted in a significant reduction of noise and biases in the FG-departures of surface sensitive channels. Assimilation of these channels seems to improve the forecast accuracy.

Bias correction over land and ocean has been separated for the AMSU-A channels 4 and 5. As a result the residual bias over land for these channels has been significantly reduced.

Influence of the residual cloud contamination, errors in the atmospheric profiles and skin temperature on the quality of the emissivity retrievals should be addressed in the future. Time sequences of the emissivity estimations over the fixed geographical locations show high variability over short periods (not shown). Using the Kalman filter to reduce the random errors in the retrievals is currently being evaluated.

## References

- Karbou, F., and C. Prigent, 2005: Calculation of microwave land surface emissivities from satellite observations: validity of the specular approximation over snow-free land surfaces. *IEEE Trans.Geosci. Remote Sensing Letters*, **2**, **3**, 311-314
- Prigent, C., F. Chevallier, F. Karbou, P. Bauer and G. Kelly, 2005: AMSU-A surface emissivities for numerical weather prediction assimilation schemes, *Journal of Applied Meteorology*, **44**, 416-126

- Auligné, T., A.P. McNally and D. Dee, 2007: Adaptive bias correction for satellite data in a numerical weather prediction system. *Q.J.R.Meteorol.Soc.*, **133**, 631-642
- Kelly, G., and P. Bauer, 2000: The use of AMSU-A surface channels to obtain surface emissivity over land, snow and ice for numerical weather prediction. *In Proceedings of 11th International TOVS Study Conference*, 167-179, Budapest, Hungary.
- Huang, H.-L. And G. R. Diak, 1992: Retrieval of nonprecipitating liquid water cloud parameters from microwave data: A simulation study. *Journal of Atmospheric and Oceanic Technology*, **9**, 354-363
- Deblonde, G. and S. English, 2000: Evaluation of FASTEM and FASTEM2 fast microwave oceanic surface emissivity model. *Proceedings of the 11th International TOVS Study Conference*, 67-78, Budapest, Hungary.

# Monitoring and Assimilation of IASI Radiances at ECMWF

Andrew Collard and Tony McNally

ECMWF

## Abstract

IASI radiances have been assimilated operationally at ECMWF since 12<sup>th</sup> June 2007. The initial configuration focussed exclusively on the use of the temperature sounding 15 $\mu$ m CO<sub>2</sub> band as this was expected to provide the greatest benefit (based on experience with AIRS). This resulted in positive impact on the forecast scores. The additional assimilation of channels from the IASI humidity band are described. Ten extra IASI humidity-sensitive channels are assimilated with an assumed observation error of 1.5K, these values being chosen on examining the impact on the analysis fit to other humidity measurements with different IASI humidity channel configurations. The weight given to these new IASI humidity observations is significantly greater than that for any other satellite instrument except for AIRS. While the impact of the observations on the analysis is to improve its agreement with independent data sources, the effect on the forecast scores for relative humidity, geopotential and vector wind is found to be neutral.

## 1. Introduction

The first of the IASI (Infrared Atmospheric Sounding Interferometer) series (Chalon *et al.*, 2001) was launched on the MetOp-A satellite on 19<sup>th</sup> October 2006. IASI is an infrared Fourier transform spectrometer and is the first such instrument to fly as part of an operational meteorological mission. A series of three MetOp missions make up the EUMETSAT Polar System (EPS) which will fly in the 09.30 (descending node) polar orbit as part of the International Joint Polar System (IJPS).

IASI measures the radiance emitted from the Earth in 8461 channels covering the spectral interval from 645–2760cm<sup>-1</sup> at a resolution of 0.5cm<sup>-1</sup> (apodised). The instrument scans through 60 scan positions up to 47° either side of nadir. At each scan position observations are made in a 2x2 array of fields of view each with a diameter 1.25°, corresponding to 12km at nadir.

High spectral-resolution infrared sounders such as IASI can provide information on the atmospheric state with a vertical resolution of the order of 1km (e.g., Prunet *et al.*, 1998; Collard, 1998) – far superior to other nadir sounding instruments. The vertical resolution is a result of high quality measurements made with a large number of channels with different, overlapping Jacobians.

IASI observations have been disseminated in near-real-time to selected NWP centres since February 2007 and were declared operational on 27<sup>th</sup> July 2007. All IASI data (i.e., 8461 channels and every field of view) are received at ECMWF via the EUMETCAST system.

The exploitation of IASI data at ECMWF has been based on the system used for the operational assimilation of radiances from the Atmospheric Infrared Sounder (AIRS) instrument since September 2003 (McNally *et al.*, 2006). AIRS (Aumann *et al.*, 2003), unlike IASI and future operational advanced infrared sounders such as CrIS, is a grating spectrometer rather than an interferometer but has similar spectral and spatial coverage and resolution to IASI. The experience with the operational use of AIRS data for the five years preceding IASI has facilitated the efficient implementation of an operational system for assimilation of IASI observations as described in this paper.

In this paper the initial implementation of IASI data assimilation is reviewed and the introduction of IASI humidity data is discussed. The impact of the assimilation of these channels on the forecast

fields is described and based on the results it is proposed to modify the use of both AIRS and IASI humidity channels in the ECMWF data assimilation system.

## 2. Initial Assimilation of IASI Radiances.

The initial configuration for the assimilation of IASI radiances is described in Collard and McNally (2008). This initial implementation uses 168 channels in the 15 $\mu$ m CO<sub>2</sub> band. Fields of view over land not used nor are channels affected by cloud. The density of channels chosen in the upper-troposphere/lower-stratosphere region is close to the maximum possible once channels with interfering species are omitted and adjacent channels are not used due to high correlations caused by apodisation (Collard, 2007). The distribution of the used channels is shown in Figure 1, where it can be seen that the density of channels used in IASI assimilation is much larger than that for AIRS. The impact of assimilating these channels is shown in Figure 2 where the forecasts are verified versus the operational analysis at the time which did not contain information from IASI. There is significant positive impact in the medium-range.

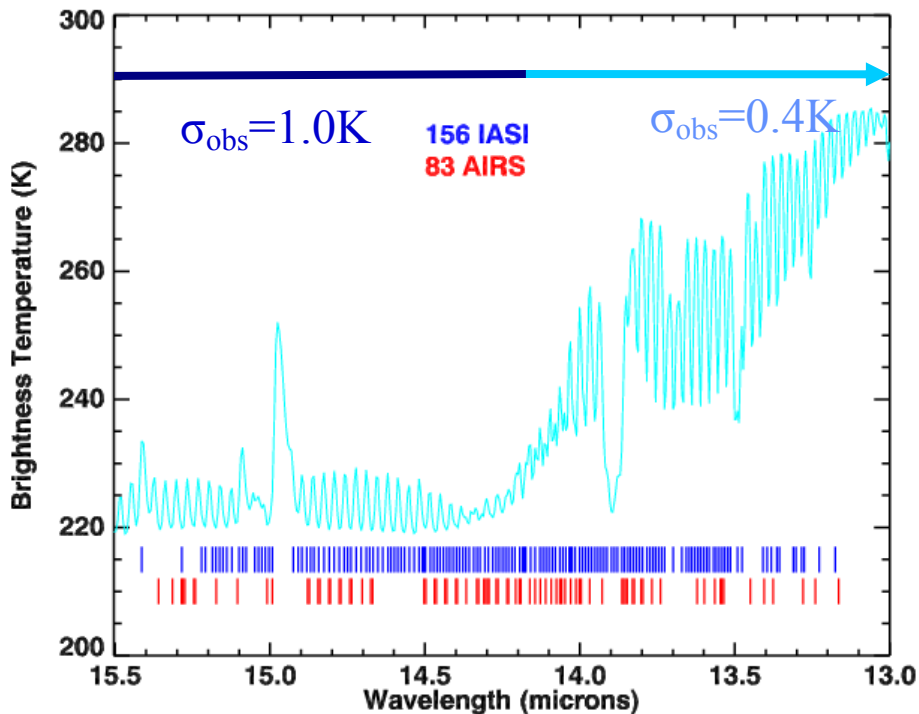
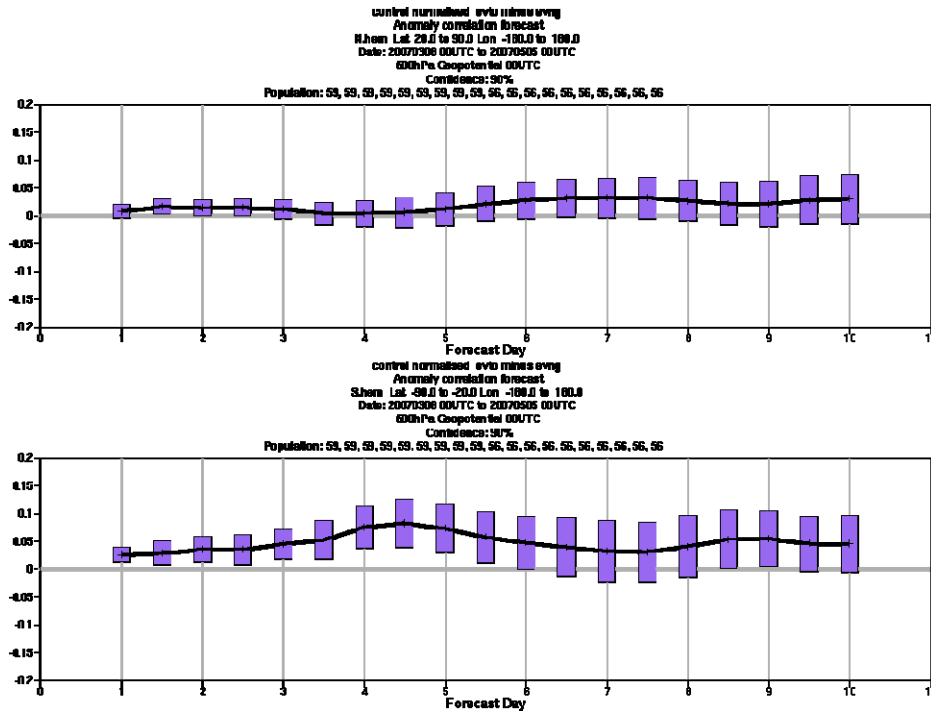


Figure 1: The 15 $\mu$ m CO<sub>2</sub> band of a typical IASI spectrum showing the positions of the channels actively used in AIRS and IASI assimilation. Also indicated are the observation errors assigned for both instruments.



**Figure 2: Change in anomaly correlation forecast scores on assimilating IASI radiances for northern (top) and southern (bottom) hemisphere geopotential at 500hPa. The scores are normalised by the control’s forecast error and positive values indicate improvement on using IASI.**

### 3. Addition of IASI Humidity Channels.

#### 3.1. Cloud detection

AIRS and IASI use the McNally and Watts (2003) cloud detection scheme which is employed to identify channels which are unaffected by cloud. This algorithm works by taking the observed-minus-calculated brightness temperature differences (hereinafter also referred to as first guess departures) and looking for the signature of opacity that is not included in the clear-sky calculation (i.e. cloud or aerosol). To do this, the channels are first ordered according to their height in the atmosphere (with the highest channels first and the channels closest to the surface last) and then the resulting ranked brightness temperature departures are smoothed with a moving-average filter in order to reduce the effect of instrument noise. The level at which cloud no longer significantly affects the radiances is found by stepping through the channels in order of increasing height until the first-guess departure and local gradient fall below pre-determined thresholds. All channels below this point are marked as cloudy and all channels above as clear. The thresholds are set to conservative values to reduce the possibility of cloud-contaminated radiances being used.

The current operational configuration for AIRS at ECMWF employs a “in-band” configuration of cloud detection scheme which divides the spectrum into five bands and uses the first guess departures in each band to determine the clear channels therein. A feature of this scheme is that in the water band large humidity errors may be interpreted as clouds and such observations may be rejected accordingly. A more realistic distribution of first-guess departures in the humidity band can be obtained by using the Watts & McNally cloud detection scheme in the 15 $\mu$ m temperature sounding CO<sub>2</sub> band and using the cloud height derived there to infer clear channels in the humidity band (this method is hereinafter referred to as “cross-band cloud detection”). This approach has not been

operationally implemented for AIRS before the present as the impact on forecast scores is negative unless the assumed 2.0K observation errors are inflated significantly.

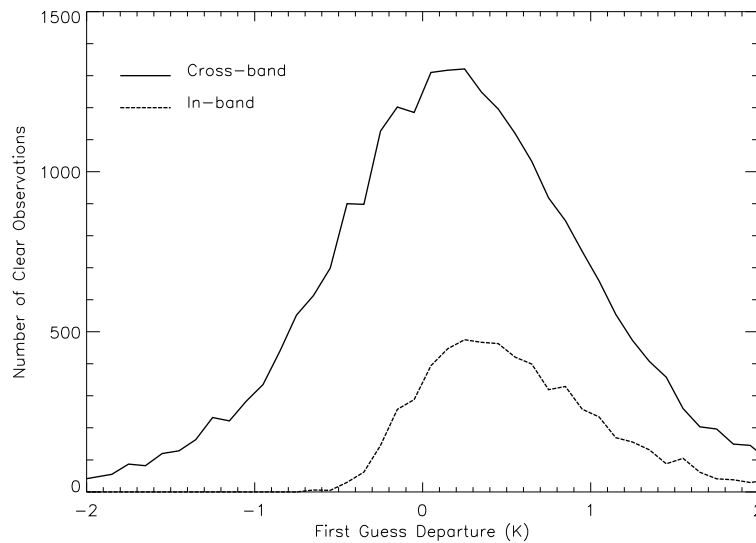


**Figure 3: The histogram of the first guess departures for AIRS channel 1477 when using in-band and cross-band cloud detection.**

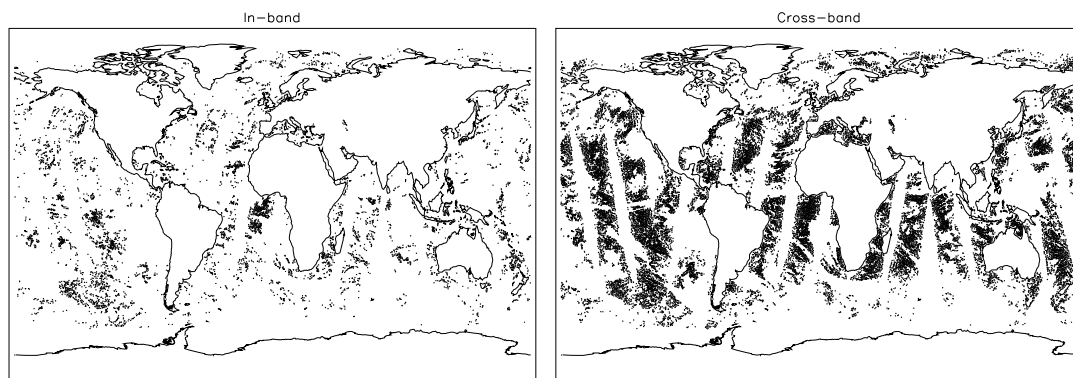


**Figure 4: The distribution of clear fields of view for AIRS channels 1477 as determined by in-band (left) and cross-band (right) cloud detection configurations.**

The difference between the “in-band” and “cross-band” configurations is illustrated in Figures 3 and 4. Here the distribution of clear observations and the histogram of observed-background brightness temperature differences are shown for AIRS channel 1477 ( $1345.31\text{cm}^{-1}$ ;  $7.433\mu\text{m}$ ) which peaks around 600hPa. The cross-band scheme can be seen to provide a more symmetric probability distribution function (with a standard deviation more consistent with that expected from background model error) and far better global coverage. For these reasons, the cross-band configuration will be used for the active use of IASI humidity channels.

### 3. Channel selection and assumed observation errors.

To put the discussion of IASI observation errors into context, Figure 5 shows the mean and standard deviation of observed-background brightness temperature for all IASI channels in clear fields of view (the clear fields-of-view are determined by an independent test based on the homogeneity of the scene as seen by AVHRR channel 5 – an infrared window channel). It can be seen that the standard deviation in the  $6.3\mu\text{m}$  humidity band (between  $1350$  and  $2000\text{cm}^{-1}$ ) is around 1.7K. Except for the highest peaking channels on the shorter wavelength side of the band (seen as positive spikes between  $1750$  and  $2000\text{cm}^{-1}$ ), this signal is dominated by errors in the background humidity. On the

“longward” side of the band ( $1350$  and  $1600\text{cm}^{-1}$ ), where the majority of the channels selected for monitoring are situated, instrument noise is in the  $0.2\text{K}$ - $0.5\text{K}$  range. The situation is very similar for AIRS except the shortwave side of the humidity band is missing and the instrument noise is slightly lower.

The current assumed observation error for AIRS humidity channels is  $2.0\text{K}$  (with the in-band cloud detection reducing the total weight given to the band further). Experiments with the adjustment of this observation error have shown that the fit to other observations (see below for explanation of this in the context of IASI) is degraded if the observation error is reduced further.

For IASI, the decision has been made to implement a system using cross-band cloud detection and to derive reasonable values for the number of channels used and the assumed observation errors. Two channel configurations were tested. The first used all humidity channels in the 366 channel set that have no significant signal from the stratosphere and above, resulting in 86 channels being used. The second channel configuration used a subset of 10 channels chosen to sample as much of the troposphere as possible. The humidity Jacobians for these channels are shown in Figure 6. A number of experiments were run (for five days) where the assumed observation error in the humidity band was varied. The degree to which the analysis fit to other satellite observations was improved or degraded (relative to the case where no extra channels were used) was then examined. The results are presented in Figures 7 and 8 where it can be seen that in both cases the fit to other observations is improved with decreasing assumed observation error until a point is reached beyond which the fit is degraded. By this measure the best observation error to assume for the 86 channel case is around  $4\text{K}$  whereas if 10 channels are used this value is reduced to  $1.5\text{K}$ .

Based on these experiments the decision was made to explore initially the implementation of ten IASI humidity channels with a  $1.5\text{K}$  error assumed.

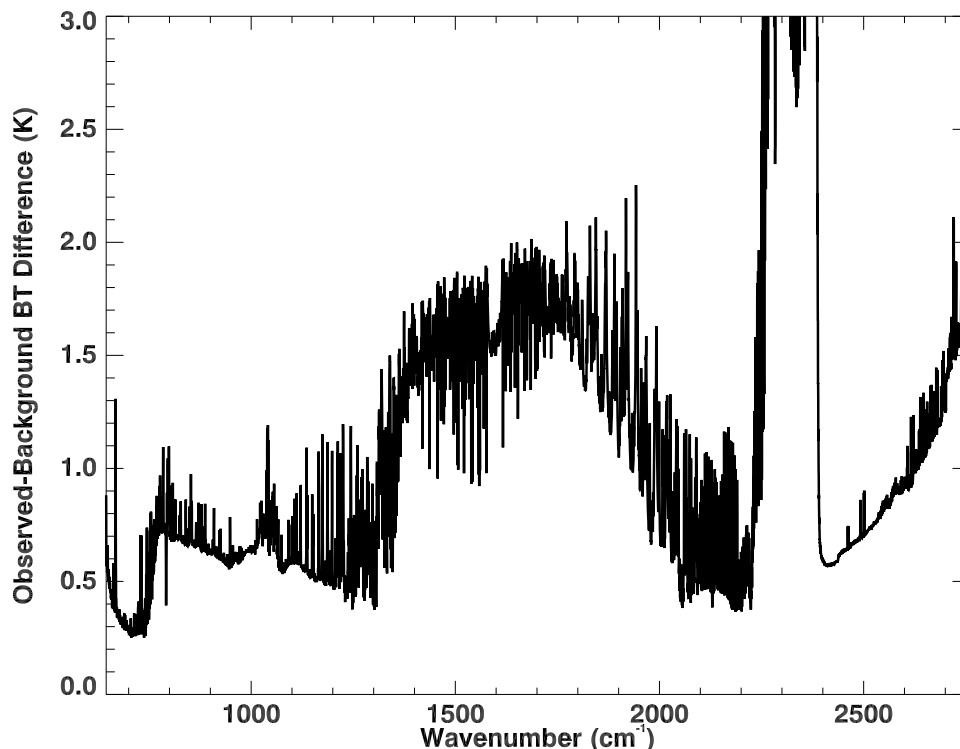


**Figure 5: The standard deviation of the observed-minus-background brightness temperature differences for clear IASI fields of view over sea. Clear scenes were identified through the homogeneity of AVHRR Channel 5 in the IASI field of view. The standard deviation of the departures in the humidity band (between  $1350$  and  $2000\text{cm}^{-1}$ ) is  $\sim 1.7\text{K}$  and is dominated by NWP model error.**

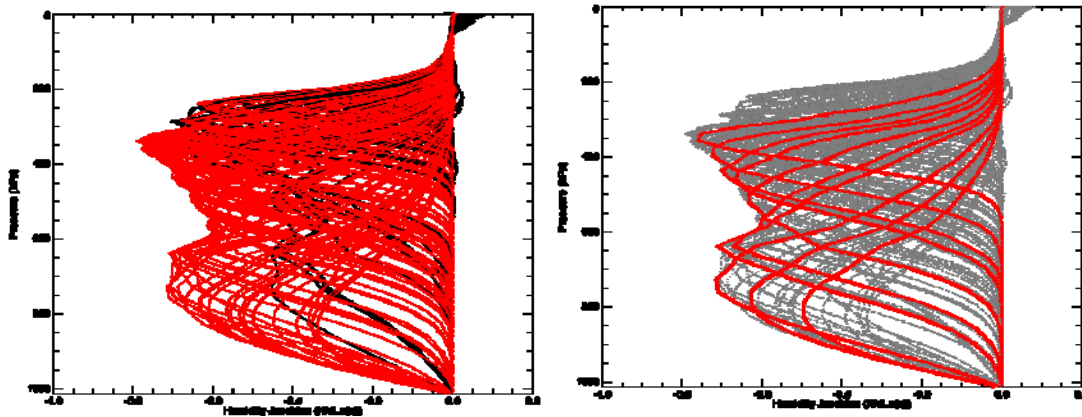


Figure 6: The humidity jacobians for the 86 (left) and 10(right) extra channels tested. The black curves in the left-hand plot are those channels from the 366 monitored channels that are not included in the 86. The grey curves in the right hand plot are the Jacobians for all unused IASI channels in the humidity band.

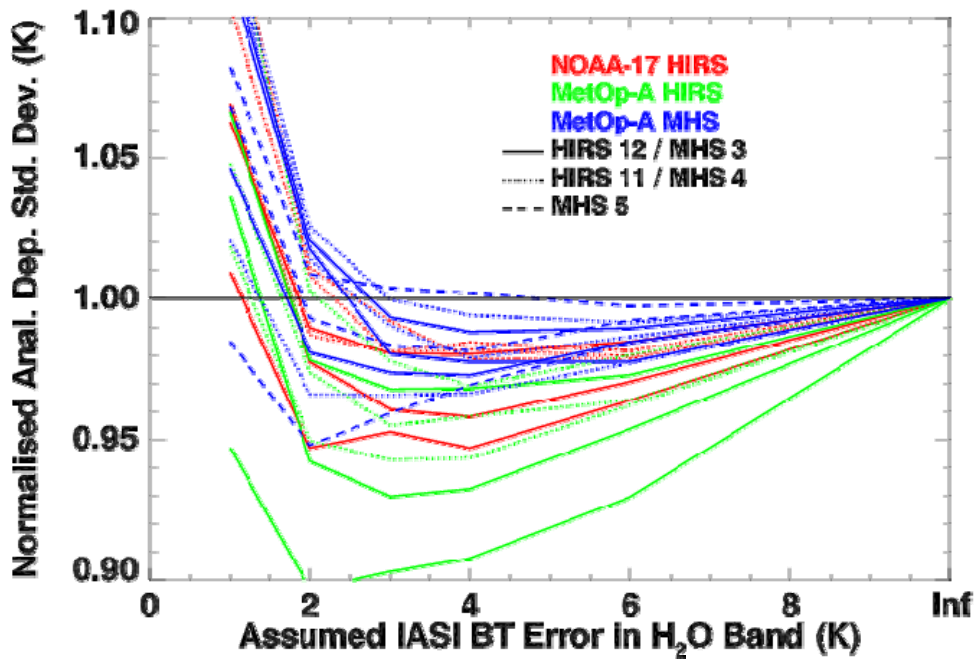


Figure 7: Change in the fit of the analysis to other satellite observations as the assumed observation error for 86 channels in the IASI humidity band is varied. The analysis departures are normalised by the analysis departures when the IASI humidity band is not assimilated.

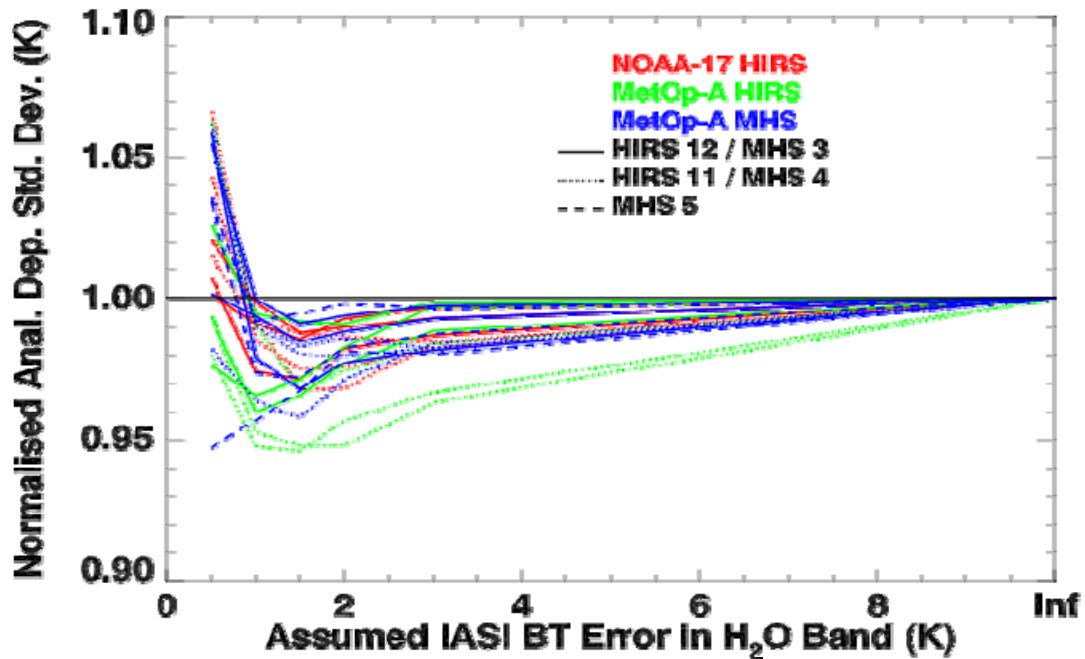


Figure 8: As Figure 7 but for 10 channels.

### 3.2. Active use of IASI radiances

An experiment was run using CY32R3 at T511 covering the period from 1<sup>st</sup> August 2007 to 23<sup>rd</sup> September 2007 employing the extra IASI humidity channels, plus a similar control experiment without the extra channels. As would be expected from the initial experiments described in the previous section, the improvement in the fit to other humidity observations is marked.

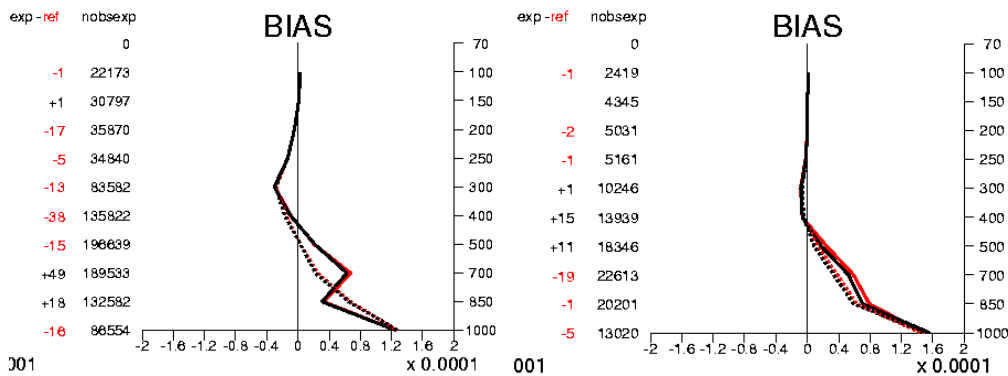
Table 1 shows how the fits to the analysis of a number of humidity sensitive satellite observations are improved when the extra IASI channels are assimilated. The three instruments which are affected most are shown; two of these being on the same platform as IASI while the third is on NOAA-17 which has a similar equator crossing time. Figure 9 shows an improvement in the fit to the specific humidities measured by radiosondes.

Figure 10 shows a cross section of the difference in the RMS relative humidity increments between the experiment and the control for the one-month period starting from 14<sup>th</sup> August. In both the experiment and control the RMS RH increments are of the order of 5% globally. The addition of IASI humidity channels increases this value by up to 0.5% in the mid-troposphere, particularly in the extra-tropical southern hemisphere. Inspection of the 500hPa level (Figure 11) shows, as expected, that the increments are confined to the oceans as IASI humidity channels are not assimilated over land or sea-ice.

Temperature changes due to the inclusion of IASI humidity channels are found to be very small (~0.01K).

Area	Instrument	Chan.	Root Mean Square First Guess Departures (K)			Root Mean Square Analysis Departures (K)		
			Expt	Cntl	% Diff	Expt	Cntl	% Diff
N.Hemis.	MetOp MHS	3	1.701	1.704	-0.2	1.147	1.168	-1.8
		4	1.527	1.529	-0.1	1.053	1.071	-1.7
		5	1.326	1.336	-0.7	1.019	1.040	-2.0
	NOAA-17 HIRS	11	0.870	0.878	-0.9	0.535	0.550	-2.7
		12	1.135	1.141	-0.5	0.825	0.836	-1.3
	MetOp HIRS	11	0.864	0.871	-0.8	0.537	0.560	-4.1
12		1.135	1.139	-0.4	0.816	0.832	-1.9	
Tropics	MetOp MHS	3	1.902	1.909	-0.4	1.113	1.134	-1.9
		4	1.589	1.597	-0.5	0.960	0.995	-3.5
		5	1.341	1.350	-0.7	0.919	0.956	-3.9
	NOAA-17 HIRS	11	0.941	0.951	-1.1	0.488	0.503	-3.0
		12	1.427	1.436	-0.6	0.838	0.847	-1.1
	MetOp HIRS	11	0.932	0.936	-0.4	0.490	0.520	-5.8
12		1.449	1.459	-0.7	0.835	0.860	-2.9	
N.Hemis.	MetOp MHS	3	1.728	1.740	-0.7	1.082	1.113	-2.8
		4	1.537	1.548	-0.7	1.035	1.057	-2.1
		5	1.343	1.353	-0.7	1.079	1.093	-1.3
	NOAA-17 HIRS	11	0.926	0.935	-1.0	0.578	0.593	-2.5
		12	1.309	1.316	-0.5	0.899	0.916	-1.9
	MetOp HIRS	11	0.916	0.922	-0.7	0.569	0.600	-5.2
12		1.313	1.321	-0.6	0.888	0.920	-3.5	

**Table 1: Changes in data fits for humidity-sensitive channels on adding ten IASI humidity channels. Negative differences indicate an improvement.**



**Figure 9: Bias of first guess departures for northern (top) and southern hemisphere (bottom) radiosonde specific humidities. The black curve is the experiment with the extra IASI humidity channels, the red is the control. Solid lines are observed-background differences and dotted lines are observed-analysis differences.**

Average of rel hum 20070814 2100 step 0 Expver F010 (180.0W-180.0E)

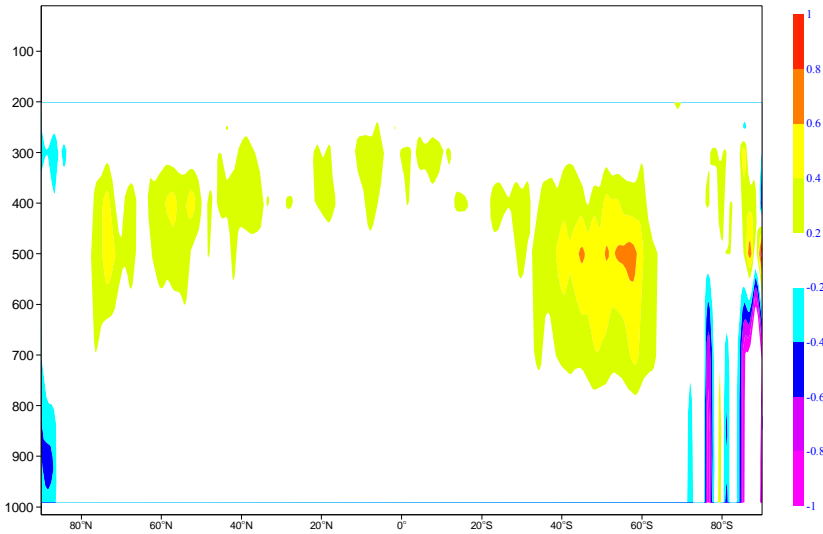


**Figure 10: Zonal average of the difference in RMS analysis relative humidity increments (in percent) between experiments with and without 10 additional IASI humidity-sensitive channels. Positive values indicate that RMS increments are larger when the additional channels are used. The statistics are the one month period between 14<sup>th</sup> August and 14<sup>th</sup> September 2007. For comparison, the absolute RMS relative humidity increment is typically 5%.**

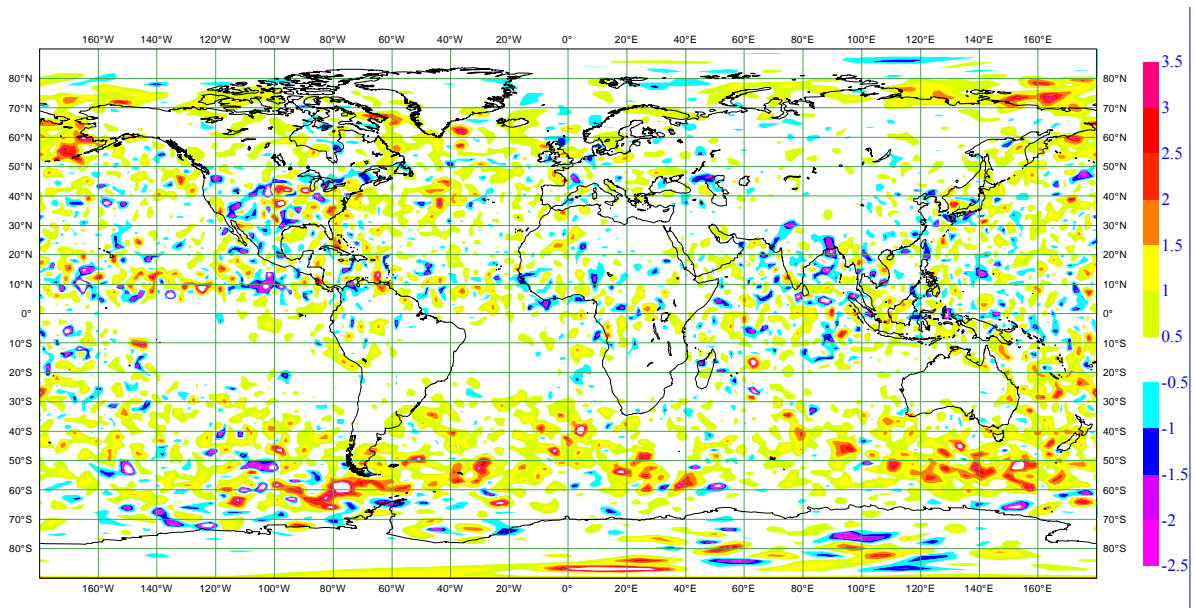


**Figure 11: As Figure 10 but the 500hPa field.**

### 3.3 Impact of IASI on forecasts

Figure 12 shows the forecast verification scores for relative humidity verified versus the operational analysis and normalised by the forecast error of the control experiment. Shown are the zonal scores for the 500hPa as this is where the greatest impact on the analysis was found (although the situation is similar for other levels). The impact of the assimilation of the IASI water vapour channels can be seen to be essentially neutral except for the very shortest ranges where the small negative signal may be attributed to the effect of verifying versus an analysis that omits the information from the extra channels. It should be noted that the signal at short-range is magnified by the small normalising factor (the absolute forecast error).

The magnitude and sign of the forecast error differences at the shortest range are highly dependent on the form of the verifying dataset. Figure 13 illustrates this through a comparison of the zonally averaged root mean square 24 hour forecast error differences for relative humidity for three verifying analyses. The first has both the experiment and control verified by the operational analysis (which does not include the additional IASI humidity information). The second is verified by the own analyses of the experiment and control; this is the only one of the three where the verifying controls are different. The third uses the experiment with the extra IASI channels to provide the verifying analysis. The fits to independent data discussed in the previous section indicate that this final analysis probably has the most realistic humidity fields (in that they incorporate the additional information provided by IASI) and the forecast verifications in this case are favourable but these results are best interpreted as showing that forecast verification scores at the shortest range, whether positive or negative, are not reliable.

The forecast scores for other fields are essentially neutral, as illustrated in Figures 14 and 15 for extra-tropical geopotential and tropical vector winds respectively.

In summary, the forecast impact on the addition of the extra IASI humidity-sensitive channels is neutral (if one ignores verification issues at the shortest range). The positive impact of the new channels is in the improvement to the fit of the analysed humidity field to observations independent of IASI.

In order to enforce consistency between AIRS and IASI, an additional experiment has been run where AIRS the cloud-detection in the humidity band has been changed to the cross-band configuration and seven channels in the AIRS water band are active, each with an assumed observation error of 1.5K. This change has a neutral impact on forecast fields.

## **4. Summary**

IASI data have been actively assimilated at ECMWF since 12<sup>th</sup> June 2007. The initial configuration focussed on 168 channels in the 15 $\mu$ m CO<sub>2</sub> band and positive impact was demonstrated in the extra-tropical geopotential forecast fields.

Active assimilation of IASI humidity channels has been introduced. The chosen configuration uses cross-band cloud detection and allows the assimilation of up to ten channels from the 6.3 $\mu$ m water band (depending on cloud conditions) with an assumed observation error of 1.5K as by examining the fit to other independent observations. A similar configuration for AIRS with seven channels has been introduced for consistency. It should be noted that the total weight given to the IASI and AIRS humidity observations is significantly greater than for any other satellite instrument. The impact of these observations on the analyses from a full data assimilation system is to significantly reduce the fit to other humidity-sensitive measurements in the vicinity of the IASI observations. The forecast impacts are essentially neutral if one disregards the shortest ranges where verification is problematic.

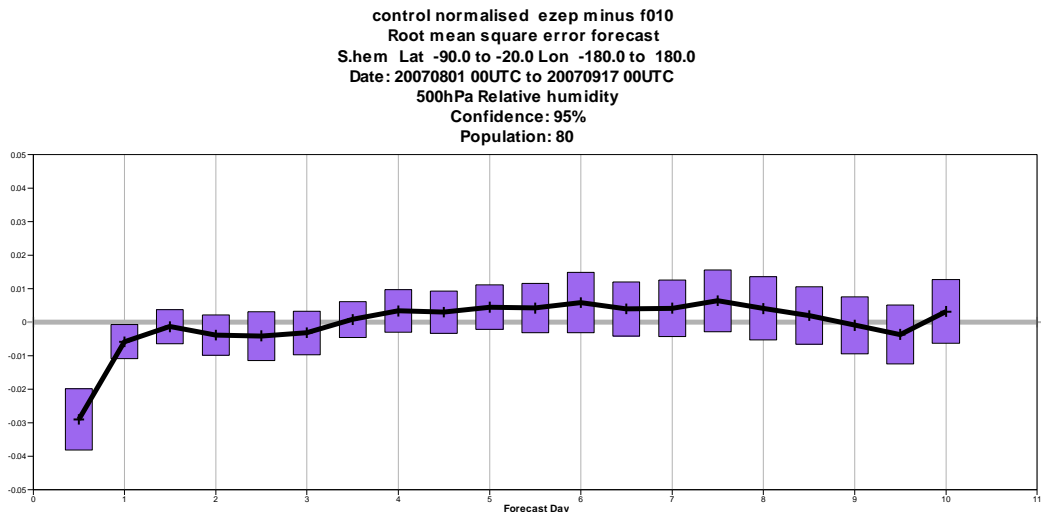
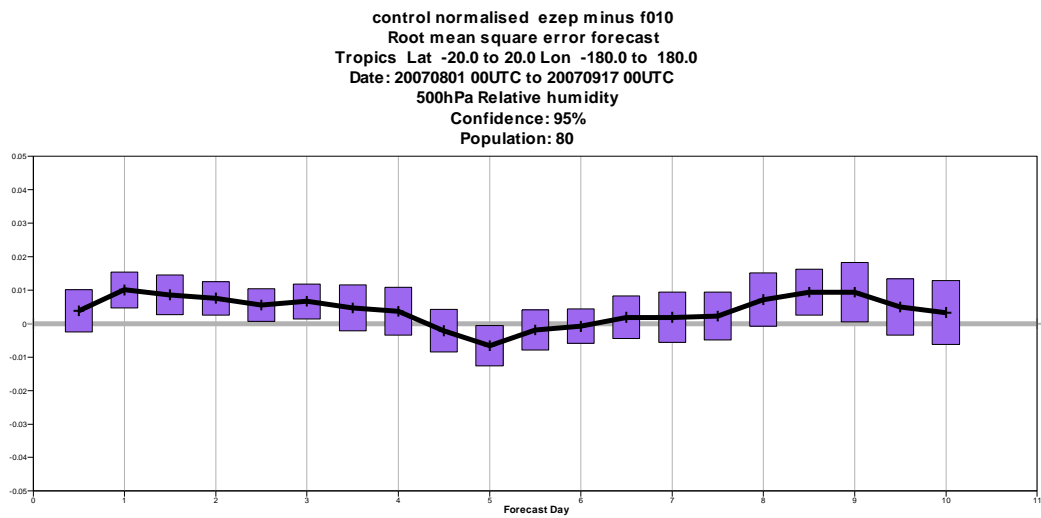
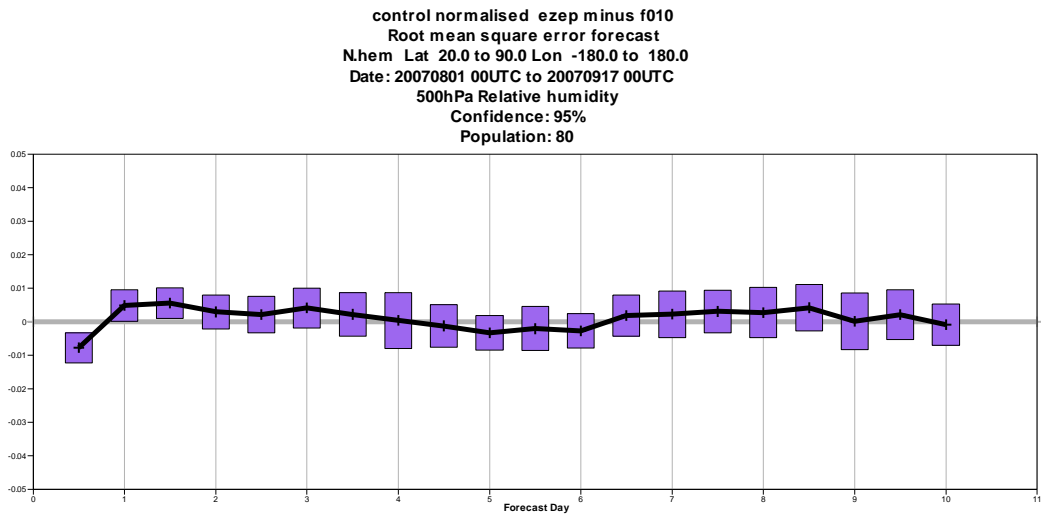


**Figure 12: Forecast error differences for relative humidity at 500hPa for northern hemisphere extra-tropics (top), the tropics (middle) and southern hemisphere extra-tropics (bottom) on assimilating 10 additional IASI humidity channels. The scores are rms differences and are normalised by the rms forecast error of the control run and are verified versus operations. Positive values indicate an improvement in forecast skill.**

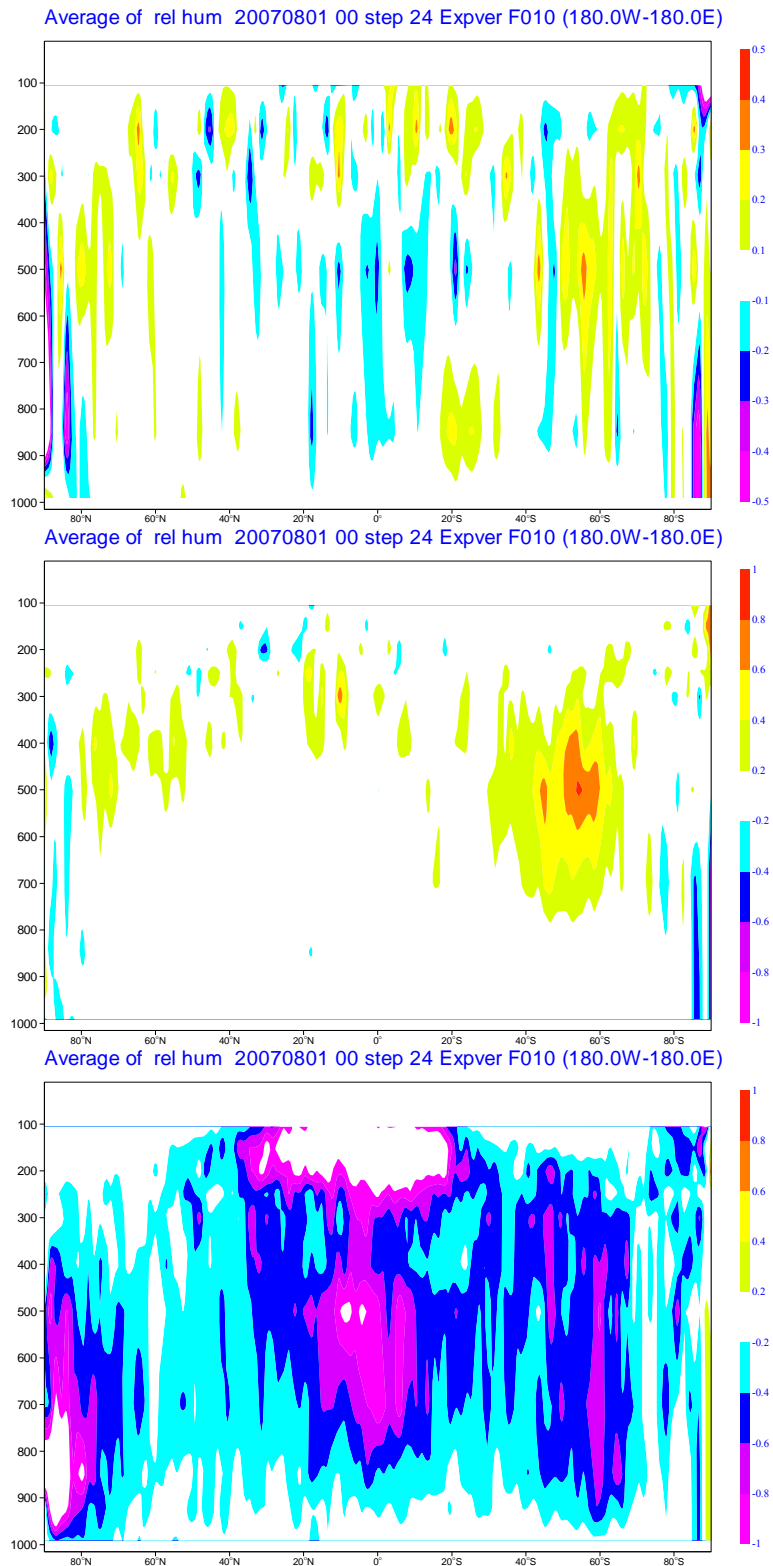


**Figure 13: Zonal average of forecast error differences at 24 hours on assimilating 10 IASI channels for relative humidity. Positive values indicate degradation in forecast skill. The forecasts are verified versus the operational analysis (top), own analysis (middle) and the analysis from the experiment with the additional IASI humidity channels (bottom).**

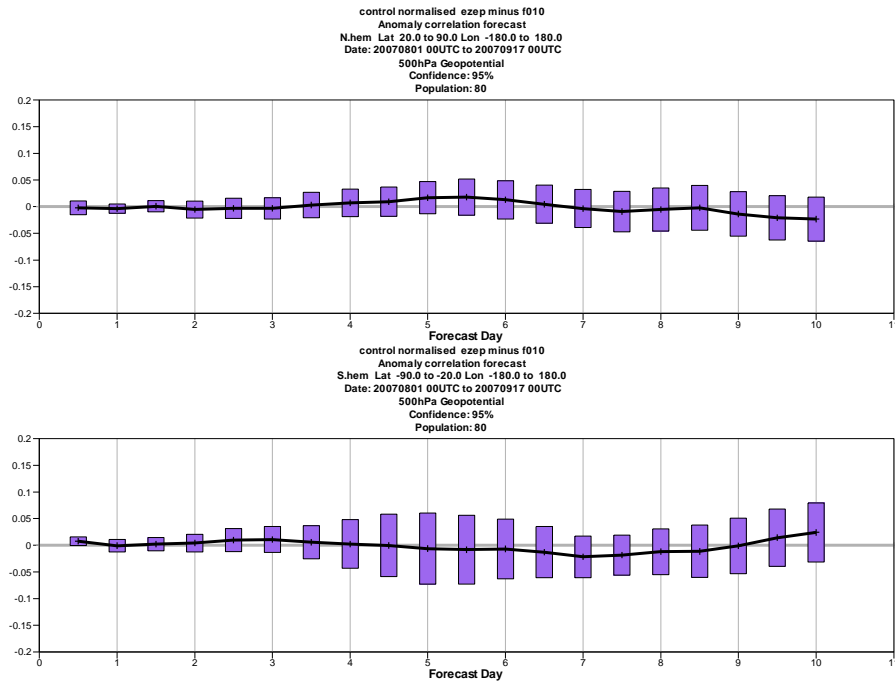


**Figure 14: Forecast error differences for geopotential at 500hPa for northern (top) and southern hemisphere extra-tropics on assimilating an additional 10 IASI humidity channels. The scores are rms differences and are normalised by the rms forecast error of the control run and are verified versus operations. Positive values indicate an improvement in forecast skill.**

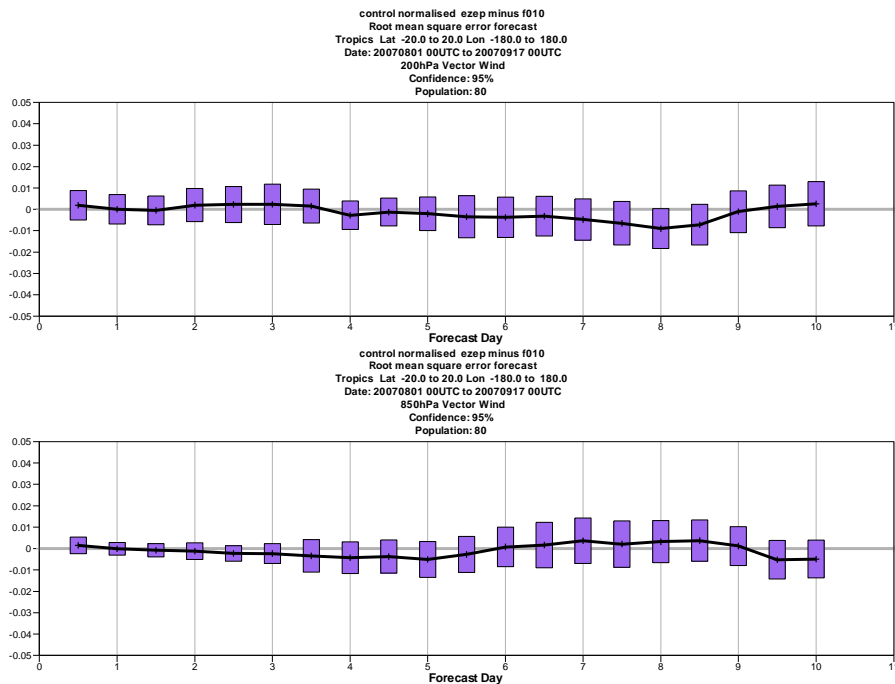


**Figure 15: Forecast error differences for tropical vector winds at 200hPa (top) and 850hPa extra-tropics on assimilating an additional 10 IASI humidity channels. The scores are rms differences and are normalised by the rms forecast error of the control run and are verified versus operations. Positive values indicate an improvement in forecast skill.**

## References

Aumann H.H., Chahine M.T., Gautier C., Goldberg M.D., Kalnay E., McMillin L.M., Revercomb, H., Rosenkranz P.W., Smith W.L., Staelin, D.H., Strow L.L. and Susskind J. (2003). AIRS on the Aqua

mission: Design, science objectives, data products, and processing systems. *IEEE Trans. Geosci. and Remote Sensing*, **41**, 253-264.

Chalon G., Cayla F. and Diebel D. (2001). IASI: An Advanced Sounder for Operational Meteorology. *Proceedings of the 52<sup>nd</sup> Congress of IAF, Toulouse France, 1-5 Oct. 2001*.

Collard, A.D. (1998). Notes on IASI Performance. *United Kingdom Meteorological Office, Numerical Weather Prediction Branch Technical Note, No. 253*.

Collard, A.D. (2007). Selection of IASI channels for use in numerical weather prediction. *Q.J.R. Meteorol. Soc.*, **133**, 1977-1991.

Collard, A.D. and A.P. McNally (2008). Assimilation of IASI Radiances at ECMWF. *Submitted to Q.J.R. Meteorol. Soc.*

Kelly, G. and J.-N. Thépaut (2007). Evaluation of the impact of the space component of the Global Observing System through Observing System Experiments. ECMWF Newsletter No. 112, Autumn 2007.

McNally, A.P. and P.D. Watts (2003). A cloud detection algorithm for high-spectral-resolution infrared sounders. *Q.J.R. Meteorol. Soc.*, **129**, 3411-3423.

McNally A.P., Watts, P.D., Smith J.A., Engelen R., Kelly G.A., Thépaut J.N. and Matricardi M. (2006). The assimilation of AIRS radiance data at ECMWF. *Q.J.R. Meteorol. Soc.*, **132**, 935-957.

## **Appendix A**

IASI humidity channels used:

2889,2958,2993,3002,3049,3105,3110,5381,5399 and 5480

AIRS humidity channels used:

1329, 1424, 1466, 1471, 1520, 1565 and 1740

# **3<sup>rd</sup> Annual Passive Sensing Microwave Workshop**

## **Proceedings/Summary**

***David McGinnis***

*National Environmental Data Information Service*

*Silver Spring, MD, US*

***Richard Kelley***

*Computer Sciences Corporation for NOAA/NESDIS*

*National Satellite Operations Facility, Suitland, MD, US*

The efforts of the (international) Space Frequency Coordination Group (SFCG) and International Telecommunication Union-Radiocommunication Sector (ITU-R) prompted the conduct of a NOAA Passive Sensing Workshop in 2007. The workshop's objective was to finalize the results of two previous workshops. It also focused on the introduction and discussion of technical papers on the identification, evaluation and utilization of particular passive sensing microwave bands, emphasizing bands above 275 GHz. This paper summarizes the workshop, describes ITU-R recommendations which relate to passive sensing (RS.515, RS.1028, and RS.1029) and provides a table which is an initial guide for updating the recommendations.

Workshop attendees recommended several changes and some additions to the existing table. Variables addressed were vegetation biomass, cirrus cloud, ice water path, cloud ice, cloud liquid water, height and depth of melting layer, precipitation, soil moisture, and the water vapor profile. Observations of these variables spanned the range of 1.37 to 882 GHz. It is hoped that the presentation of these workshop results will lead to discussions of needs for additional table entries as the changes to the ITU-R recommendations go forward.

A summary of the workshop along with links to papers and presentations can be found at <http://sfcgonline.org/PM%20Workshop/pmw.aspx>.

### **What is an ITU-R Recommendation?**

The ITU-R Recommendations are international technical standards developed by the Radiocommunication Sector of the ITU. They are the result of studies undertaken by Radiocommunication Study Groups on:

- the use of a vast range of wireless services, including popular new mobile communication technologies:

- the management of the radio-frequency spectrum and satellite orbits;
- the efficient use of the radio-frequency spectrum by all radiocommunication services;
- terrestrial and satellite radiocommunication broadcasting;
- radio wave propagation;
- systems and networks for the fixed-satellite service, for the fixed service and the mobile service;
- space operation, Earth exploration-satellite,
- Meteorological-satellite and radio astronomy services.

The ITU-R Recommendations are approved by ITU Member States. Their implementation is not mandatory; however, as they are developed by experts from administrations, operators, and the industry and other organizations dealing with radiocommunication matters from all over the world, they enjoy an esteemed reputation and are implemented worldwide.

### **What are the three ITU-R Recommendations of concern?**

1. RS. 515 recommends frequency bands and associated bandwidths for passive sensing of the Earth's land, oceans and atmosphere. See the appendix to this paper for a table of requirements for passive sensing of environmental data
2. RS. 1028 recommends performance criteria in the form of measurement sensitivities and data availability for passive remote sensing of the Earth's land, oceans and atmosphere. See the appendix to this paper for the performance criteria and a description of terms used therein.

3. RS. 1029

a. recommends

i. That interference levels for space borne passive sensors of environmental data should be set at 20% of the radiometer threshold

ii. Permissible interference levels and reference bandwidths for the frequency bands preferred for passive sensing of the Earth’s land, oceans and atmosphere. Levels and bandwidths are given in a table of interference criteria.

iii. That the interference level in the table should not be exceeded for more than a specified percentage of either sensor viewing area or measurement time.

b. Provides a table of values for these parameters. This table is reproduced in the appendix to this paper.

**What changes did the 3<sup>rd</sup> passive microwave workshop recommend?**

Workshop attendees represented these agencies: CNES, Environment Canada, Joint Center for Satellite Data Assimilation, Meteo France, NASA, National Academies of Sciences, National Science Foundation, NOAA/NESDIS, NPOESS-IPO, and the UK Met Office. A table of changes to the aforementioned recommendations was developed and is presented here.

Table 1: “Change Table” Updating RS.515, RS.1028, RS.1029

Band (Upper and Lower bound)	Change Status (e.g., New, Modified, etc)	Measurement and Comments (Measurement function, priority, dependencies, alternatives/comparisons, etc.)	Performance		Scan Mode (N,L)	Source (1)
			Sensitivity (K)	Data Availability		
1.37-1.4 1.4-1.427	M	Vegetation <del>index</del> <u>biomass</u> (replace)			N	JP
2.64-2.655 2.655-2.69 2.69-2.7	M	Vegetation <del>index</del> <u>biomass</u> (replace)			N	JP
4.2-4.4 4.95-4.99	M	Soil moisture Soil moisture			N	JP
6.425-7.25	M	Soil moisture			N	JP
52.6-59.3	M	Cloud liquid water			N	MD
50.2-50.4	M	Cloud liquid water			N	MD
86-92	M	Cloud liquid water			N	MD

Band (Upper and Lower bound)	Change Status (e.g., New, Modified, etc)	Measurement and Comments (Measurement function, priority, dependencies, alternatives/comparisons, etc.)	Performance		Scan Mode (N,L)	Source (1)
			Sensitivity (K)	Data Availability		
100-102	M	Precip. over sea and land			N	MD
115.25- 122.25	M	Cloud liquid water, precip. over sea and land, incl. light precip. and snowfall, ht. and depth of melting layer			N	MD
164-167	M	Water vapor profile, precip. over land and snowfall			N	MD
174.8- 191.8	M	Snowfall, cloud ice water path retrieval			N	MD
239-247 241.7- 244.7	N	Quasi window for cirrus clouds and cloud ice (Can the window, currently in Rec. 515-4, at 226-231.5 GHz be used? Avoid spectral lines)			N	JP MD
316-334	M	Cloud ice			N	JP
334-336	N	Cloud ice, Cirrus, quasi-window			N	JP
371-389	M	Cloud ice			N	JP
446.5- 449.5 439.3- 456.7	N	Cloud ice water path (integrated ice in clouds) and cirrus			N	MD JP
634.8- 637.6	M	Cloud ice			N	JP
648.2- 651.0	M	Cloud ice, paired with 634.8-637.6 GHz, note Rec. 515-4 already has 634-654 GHz			N	JP
662.5- 666.5	N	Cirrus clouds and cloud ice water path			N	MD
866-882	N	Cloud ice			N	JP

## Notes

(1) JP:Jeff Piepmeier NASA/GSFC

MD: Markus Dreis EUMETSAT

## **What next?**

The next meeting of the ITU's World Radiocommunication Conference will be held in 2011. Changes and additions to existing recommendations will be considered during this meeting. The frequency spectrum above 275 GHz is unregulated at this writing. As scientists, it is important to make our voices heard by advising ITU participants of our interests and concerns. One way of making our voices heard is to provide national ITU representatives with updates to tables presented in this paper. If the reader needs to know how to contact their national representative, just speak to either of the authors:

Dave McGinnis: 1.301.713.3104 x 149 (work) or [Dave.McGinnis@noaa.gov](mailto:Dave.McGinnis@noaa.gov)

Rich Kelley: 1.301.817.4636 (work) or [Richard.Kelley@noaa.gov](mailto:Richard.Kelley@noaa.gov)

**Appendix: Tables from RS. 515-4, RS. 1028-2, RS. 1029-2**

**Table: Requirements for passive sensing of environmental data, from RS. 515-4**

Frequency band(s) <sup>(1)</sup> (GHz)	Total bandwidth required (MHz)	Spectral line(s) or centre frequency (GHz)	Measurement	Scan mode N, L <sup>(2)</sup>
1.37-1.4s, 1.4-1.427P	100	1.4	Soil moisture, ocean salinity, sea surface temperature, vegetation index	N
2.64-2.655s, 2.655-2.69s, 2.69-2.7P	45	2.7	Ocean salinity, soil moisture, vegetation index	N
4.2-4.4s, 4.95-4.99s	200	4.3	Sea surface temperature	N
6.425-7.25	200	6.85	Sea surface temperature	N
10.6-10.68p, 10.68-10.7P	100	10.65	Rain rate, snow water content, ice morphology, sea state, ocean wind speed	N
15.2-15.35s, 15.35-15.4P	200	15.3	Water vapour, rain rate	N
18.6-18.8p	200	18.7	Rain rates, sea state, sea ice, water vapour, ocean wind speed, soil emissivity and humidity	N
21.2-21.4p	200	21.3	Water vapour, liquid water	N
22.21-22.5p	300	22.235	Water vapour, liquid water	N
23.6-24P	400	23.8	Water vapour, liquid water, associated channel for atmospheric sounding	N
31.3-31.5P, 31.5-31.8p	500	31.4	Sea ice, water vapour, oil spills, clouds, liquid water, surface temperature, reference window for 50-60 GHz range	N
36-37p	1 000	36.5	Rain rates, snow, sea ice, clouds	N
50.2-50.4P	200	50.3	Reference window for atmospheric temperature profiling (surface temperature)	N
52.6-54.25P, 54.25-59.3p	6 700 <sup>(3)</sup>	Several between 52.6-59.3	Atmospheric temperature profiling (O <sub>2</sub> absorption lines)	N
86-92P	6 000	89	Clouds, oil spills, ice, snow, rain, reference window for temperature soundings near 118 GHz	N

**Table: Performance criteria for passive remote sensing of environmental data, from RS. 1028**

Frequency band(s) <sup>(1)</sup> (GHz)	Total BW required (MHz)	Required $\Delta T_e$ (K)	Data availability <sup>(2)</sup> (%)	Scan mode (N, L) <sup>(3)</sup>
1.37-1.4s, 1.4-1.427P	100	0.05	99.9	N
2.64-2.655s, 2.655-2.69s, 2.69-2.7P	45	0.1	99.9	N
4.2-4.4s, 4.95-4.99s	200	0.3/0.05 <sup>(4)</sup>	99.9	N

6.425-7.25	200	0.3/0.05 <sup>(4)</sup>	99.9	N
10.6-10.68p, 10.68-10.7P	100	1.0/0.1 <sup>(4)</sup>	99.9	N
15.2-15.35s, 15.35-15.4P	200	0.1	99.9	N
18.6-18.8p	200	1.0/0.1 <sup>(4)</sup>	95/99.9 <sup>(4)</sup>	N
21.2-21.4p	200	0.2/0.05 <sup>(4)</sup>	99/99.9 <sup>(4)</sup>	N
22.21-22.5p	300	0.4/0.05 <sup>(4)</sup>	99/99.9 <sup>(4)</sup>	N
23.6-24P	400	0.05	99.99	N
31.3-31.5P, 31.5-31.8p	500	0.2/0.05 <sup>(4)</sup>	99.99	N
36-37p	1 000	1.0/0.1 <sup>(4)</sup>	99.9	N
50.2-50.4P	200	0.05	99.99	N
52.6-54.25P, 54.25-59.3p	6 700 <sup>(5)</sup>	0.3/0.05 <sup>(4)</sup>	99.99	N
86-92P	6 000	0.05	99.99	N
100-102P	2 000	0.005	99	L
109.5-111.8P	2 000	0.005	99	L
114.25-116.P	1 750	0.005	99	L

115.25-116P, 116.0-122.25p	7 000(5)	0.05/0.005(6)	99.99/99(6)	N, L
148.5-151.5P	3 000	0.1/0.005(6)	99.99/99(6)	N, L
155.5-158.5(7)p	3 000	0.1	99.99	N
164-167P	3 000(5)	0.1/0.005(6)	99.99/99(6)	N, L
174.8-182p, 182-185P, 185-190p, 190-191.8P	17 000(5)	0.1/0.005(6)	99.99/99(6)	N, L
200-209P	9 000(5)	0.005	99	L
226-231.5P	5 500	0.2/0.005(6)	99.99/99(6)	N, L
235-238p	3 000	0.005	99	L
250-252P	2 000	0.005	99	L
275-277	2 000(5)	0.005	99	L
294-306	12 000(5)	0.2/0.005(6)	99.99/99(6)	N, L
316-334	18 000(5)	0.3/0.005(6)	99.99/99(6)	N, L
342-349	7 000(5)	0.3/0.005(6)	99.99/99(6)	N, L
363-365	2 000	0.005	99	L
371-389	18 000(5)	0.3	99.99	N
416-434	18 000(5)	0.4	99.99	N
442-444	2 000(5)	0.4/0.005(6)	99.99/99(6)	N, L
496-506	10 000(5)	0.5/0.005(6)	99.99/99(6)	N, L
546-568	22 000(5)	0.5/0.005(6)	99.99/99(6)	N, L
624-629	5 000(5)	0.005	99	L
634-654	20 000(5)	0.5/0.005(6)	99.99/99(6)	N, L
659-661	2 000	0.005	99	L
684-692	8 000(5)	0.005	99	L
730-732	2 000(5)	0.005	99	L
851-853	2 000	0.005	99	L
951-956	5 000(5)	0.005	99	L

- (1) P: Primary allocation, shared only with passive services (No. 5.340 of the Radio Regulations); p: primary allocation, shared with active services; s: secondary allocation.
- (2) Data availability is the percentage of area or time for which accurate data is available for a specified sensor measurement area or sensor measurement time. For a 99.99% data availability, the measurement area is a square on the Earth of 2 000 000 km<sup>2</sup>, unless otherwise justified; for a 99.9% data availability, the measurement area is a square on the Earth of 10 000 000 km<sup>2</sup> unless otherwise justified; for a 99% data availability the measurement time is 24 h, unless otherwise justified.
- (3) N: Nadir, Nadir scan modes concentrate on sounding or viewing the Earth's surface at angles of nearly perpendicular incidence. The scan terminates at the surface or at various levels in the atmosphere according to the weighting functions. L: Limb, Limb scan modes view the atmosphere "on edge" and terminate in space rather than at the surface, and accordingly are weighted zero at the surface and maximum at the tangent point height.
- (4) First number for sharing conditions circa 2003; second number for scientific requirements that are technically achievable by sensors in the next 5-10 years.
- (5) This bandwidth is occupied by multiple channels.
- (6) Second number for microwave limb sounding applications.
- (7) This band is needed until 2018 to accommodate existing and planned sensors.

## *Description of terms used in performance criteria from RS. 1028*

### *Sensitivity of radiometric receivers*

Radiometric receivers sense the noise-like thermal emission collected by the antenna and the thermal noise of the receiver. By integrating the received signal the random noise fluctuations can be reduced and accurate estimates can be made of the sum of the receiver noise and external thermal emission noise power. Expressing the noise power per unit bandwidth as an equivalent noise temperature, the effect of integration in reducing measurement uncertainty can be expressed as given below:

$$\Delta T_e = \frac{\alpha(T_A + T_N)}{\sqrt{B\tau}}$$

where:

- $\Delta T_e$  : radiometric resolution (r.m.s. uncertainty in the estimation of the total system noise,  $T_A + T_N$ )
- $\alpha$  : receiver system constant,  $\geq 1$ , depending on the system design
- $T_A$  : antenna temperature
- $T_N$  : receiver noise temperature
- $B$  : spectral resolution of spectroradiometer or bandwidth of a single radiometric channel
- $\tau$  : integration time.

The receiver system constant,  $\alpha$ , is a function of the type of detection system. For total power radiometers used by Earth exploration-satellite service sensors, this constant can be no smaller than unity. In practice, most modern total power radiometers closely approach unity.

Table: Interference criteria for passive remote sensing of environmental data (from RS. 1029-2)

Frequency band(s) <sup>(1)</sup> (GHz)	Total bandwidth required (MHz)	Reference bandwidth (MHz)	Maximum interference level (dBW)	Percentage of area or time permissible interference level may be exceeded <sup>(2)</sup> (%)	Scan mode (N, L) <sup>(3)</sup>
1.37-1.4s, 1.4-1.427P	100	27	-174	0.1	N
2.64-2.655s, 2.655- 2.69s, 2.69-2.7P	45	10	-176	0.1	N
4.2-4.4s, 4.95-4.99s	200	200	-158/-166 <sup>(4)</sup>	0.1	N
6.425-7.25	200	200	-158/-166 <sup>(4)</sup>	0.1	N
10.6-10.68p, 10.68-10.7P	100	100	-156/-166 <sup>(4)</sup>	0.1	N
15.2-15.35s, 15.35- 15.4P	200	50	-169	0.1	N
18.6-18.8p	200	200	-153/-163 <sup>(4)</sup>	5/0.1 <sup>(4)</sup>	N
21.2-21.4p	200	100	-163/-169 <sup>(4)</sup>	1/0.1 <sup>(4)</sup>	N
22.21-22.5p	300	100	-160/-169 <sup>(4)</sup>	1/0.1 <sup>(4)</sup>	N
23.6-24P	400	200	-166	0.01	N
31.3-31.5P, 31.5-31.8p	500	200	-160/-166 <sup>(4)</sup>	0.01	N

Table: Interference criteria for passive remote sensing of environmental data (from RS. 1029-2) (continued)

Frequency band(s) <sup>(1)</sup> (GHz)	Total bandwidth required (MHz)	Reference bandwidth (MHz)	Maximum interference level (dBW)	Percentage of area or time permissible interference level may be exceeded <sup>(2)</sup> (%)	Scan mode (N, L) <sup>(3)</sup>
36-37p	1 000	100	-156/-166 <sup>(4)</sup>	0.1	N
50.2-50.4P	200	200	-166	0.01	N
52.6-54.25P, 54.25-59.3p	6 700 <sup>(5)</sup>	100	-161/-169 <sup>(4)</sup>	0.01	N
86-92P	6 000	100	-169	0.01	N
100-102P	2 000	10	-189	1	L
109.5-111.8P	2 000	10	-189	1	L
114.25-116P	1 750	10	-189	1	L
115.25-116P, 116-122.25p	7 000 <sup>(5)</sup>	200/10 <sup>(6)</sup>	-166/-189 <sup>(6)</sup>	0.01/1 <sup>(6)</sup>	N, L
148.5-151.5P	3 000	500/10 <sup>(6)</sup>	-159/-189 <sup>(6)</sup>	0.01/1 <sup>(6)</sup>	N, L
155.5-158.5 <sup>(7)</sup> p	3 000	200	-163	0.01	N
164-167P	3 000 <sup>(5)</sup>	200/10 <sup>(6)</sup>	-163/-189 <sup>(6)</sup>	0.01/1 <sup>(6)</sup>	N, L
174.8-182p, 182-185P, 185-190p, 190-191.8P	17 000 <sup>(5)</sup>	200/10 <sup>(6)</sup>	-163/-189 <sup>(6)</sup>	0.01/1 <sup>(6)</sup>	N, L
200-209P	9 000 <sup>(5)</sup>	3	-194	1	L
226-231.5P	5 500	200/3 <sup>(6)</sup>	-160/-194 <sup>(6)</sup>	0.01/1 <sup>(6)</sup>	N, L
235-238p	3 000	3	-194	1	L
250-252P	2 000	3	-194	1	L
275-277	2 000 <sup>(5)</sup>	3	-194	1	L
294-306	12 000 <sup>(5)</sup>	200/3 <sup>(6)</sup>	-160/-194 <sup>(6)</sup>	0.01/1 <sup>(6)</sup>	N, L
316-334	18 000 <sup>(5)</sup>	200/3 <sup>(6)</sup>	-158/-194 <sup>(6)</sup>	0.01/1 <sup>(6)</sup>	N, L
342-349	7 000 <sup>(5)</sup>	200/3 <sup>(6)</sup>	-158/-194 <sup>(6)</sup>	0.01/1 <sup>(6)</sup>	N, L
363-365	2 000	3	-194	1	L
371-389	18 000 <sup>(5)</sup>	200	-158	0.01	N
416-434	18 000 <sup>(5)</sup>	200	-157	0.01	N
442-444	2 000 <sup>(5)</sup>	200/3 <sup>(6)</sup>	-157/-194 <sup>(6)</sup>	1	N, L

Table: Interference criteria for passive remote sensing of environmental data (from RS. 1029-2) (end)

Frequency band(s) <sup>(1)</sup> (GHz)	Total bandwidth required (MHz)	Reference bandwidth (MHz)	Maximum interference level (dBW)	Percentage of area or time permissible interference level may be exceeded <sup>(2)</sup> (%)	Scan mode (N, L) <sup>(3)</sup>
496-506	10 000 <sup>(5)</sup>	200/3 <sup>(6)</sup>	-156/-194 <sup>(6)</sup>	0.01/1 <sup>(6)</sup>	N, L
546-568	22 000 <sup>(5)</sup>	200/3 <sup>(6)</sup>	-156/-194 <sup>(6)</sup>	0.01/1 <sup>(6)</sup>	N, L
624-629	5 000 <sup>(5)</sup>	3	-194	1	L
634-654	20 000 <sup>(5)</sup>	200/3 <sup>(6)</sup>	-156/-194 <sup>(6)</sup>	0.01/1 <sup>(6)</sup>	N, L
659-661	2 000	3	-194	1	L
684-692	8 000 <sup>(5)</sup>	3	-194	1	L
730-732	2 000 <sup>(5)</sup>	3	-194	1	L
851-853	2 000	3	-194	1	L
951-956	5 000 <sup>(6)</sup>	3	-194	1	L

- <sup>(1)</sup> P: Primary allocation, shared only with passive services (No. 5.340 of the Radio Regulations); p: primary allocation, shared with active services; s: secondary allocation.
- <sup>(2)</sup> For a 0.01% level, the measurement area is a square on the Earth of 2 000 000 km<sup>2</sup>, unless otherwise justified; for a 0.1% level, the measurement area is a square on the Earth of 10 000 000 km<sup>2</sup> unless otherwise justified; for a 1% level, the measurement time is 24 h, unless otherwise justified.
- <sup>(3)</sup> N: Nadir, Nadir scan modes concentrate on sounding or viewing the Earth's surface at angles of nearly perpendicular incidence. The scan terminates at the surface or at various levels in the atmosphere according to the weighting functions. L: Limb, Limb scan modes view the atmosphere "on edge" and terminate in space rather than at the surface, and accordingly are weighted zero at the surface and maximum at the tangent point height.
- <sup>(4)</sup> First number for sharing conditions circa 2003; second number for scientific requirements that are technically achievable by sensors in next 5-10 years.
- <sup>(5)</sup> This bandwidth is occupied by multiple channels.
- <sup>(6)</sup> Second number for microwave Limb sounding applications.
- <sup>(7)</sup> This band is needed until 2018 to accommodate existing and planned sensors.

# **AAPP developments and experiences with processing METOP data**

***Nigel C Atkinson<sup>\*</sup>, Pascal Brunel<sup>†</sup>, Philippe Marguinaud<sup>†</sup> and Tiphaine Labrot<sup>†</sup>***

*<sup>\*</sup> Met Office, Exeter, UK*

*<sup>†</sup> Météo-France, Centre de Météorologie Spatiale, Lannion, France*

## **Introduction**

The ATOVS and AVHRR Pre-processing Package (AAPP) is a software package maintained by the EUMETSAT Satellite Application Facility for Numerical Weather Prediction (NWP SAF). The host institute for the NWP SAF is the Met Office, with partners ECMWF, KNMI and Météo-France (see <http://www.nwpsaf.org>).

AAPP version 6.1 and the IASI Level 1 processor OPS-LRS were released to users in October 2006, shortly before the launch of MetOp-A. Since then a number of updates have been issued, as the software has been refined in the light of post-launch MetOp data. Please see the NWP SAF web site for details of the current release.

This paper describes the new features to be found in version 6 and its updates. It then describes some recent developments in an application of AAPP – the Regional ATOVS Retransmission Services (RARS). Finally we consider the extension of AAPP to new satellites such as NPP and NPOESS.

## **AAPP Capabilities**

AAPP can be used to perform level 1 processing on the following types of polar-orbiter data:

- Locally-received direct readout data (HRPT or AHRPT)
- Regional data, e.g. EARS and RARS. Normally received BUFR-encoded at level 1c, but can be level 1a or 1b.
- Global data, e.g. from NESDIS or EUMETSAT

Of the current generation of polar-orbiting satellites, the following are supported in AAPP: NOAA-15, NOAA-16, NOAA-17, NOAA-18, MetOp-A and FY-1D. The supported instruments are as follows: AMSU, MHS, HIRS, IASI, AVHRR and the FY-1D imager MVISR.

For a series of block diagrams illustrating the AAPP processing flow, see Atkinson et. al. (2006).

## **Processing of MetOp data**

During the first half of 2007 AAPP was used operationally at a number of centres (including Met Office and Météo-France) to process the MetOp direct-readout data. This included the processing of IASI using the OPS-LRS package. A detailed comparison study of IASI local processing versus global processing was performed by Marguinaud et. al. (2007); the study concluded that although there are some small differences in the radiances, the reasons for the differences are well understood and they are not expected to be significant for Numerical Weather Prediction (NWP).

Unfortunately the primary AHRPT transmitter on MetOp-A failed on 4<sup>th</sup> July 2007 and to date there has been no activation of the secondary transmitter. Nevertheless users of OPS-LRS are encouraged to keep their software up to date in order to ensure local-global consistency should it be possible to activate the secondary transmitter in the future.

Despite the lack of AHRPT, imagery from AVHRR is still available to users via the EPS global data service, with a timeliness of approximately 1.5 to 2 hours. A tool has been added to AAPP that converts the EPS format data into the AAPP level 1b format.

### Processing of FY-1D imager data

A new feature in AAPP update 6.6 (released Feb 2008) has been the ability to process direct readout data from FY-1D. AAPP takes the five AVHRR-like channels of the MVISR imager, performs calibration and geolocation tasks and creates standard AAPP-format level 1b files. MVISR has ten channels: channels 1-5 are similar to AVHRR while channels 6-10 are additional visible/near IR channels for ocean colour, water vapour and ice/snow characterisation. Centre frequencies are listed in Liu et. al. (1999).

The instrument does have some problems (channel 3 is noisy), and the quality of the calibration and navigation is not as good as it is on NOAA satellites. But the imagery is still of useful quality. For a detailed discussion of FY-1D issues, see Levin et. al., 2005.

There are no plans at present to extend AAPP to process data from the FY-3 series – which includes infrared and microwave sounders. Instead, it is hoped that the China Meteorological Administration will provide a suitable level 1 processing package. FY-3A was launched on 27 May 2008.

### Development of IASI Principal Components

As part of *atovpp*, the user has a number of options which may be used to reduce the volume of the IASI level 1 data. These include:

- Channel selection – a set of 314 channels is provided (Collard, 2007) or the user can define his own channel selection
- Spatial thinning – choose one detector out of the four, either a fixed detector or one chosen dynamically based on the variability of the mapped AVHRR pixels
- Principal components (PCs) – the eigenvectors are supplied in a data file and the user can define how many PCs to use

In AAPP update 6.6 the handling of the PCs was enhanced to be compatible with the software package developed at ECMWF for the generation of the eigenvectors from a training set of spectra. This package is to be released as an NWP SAF deliverable.

The basic steps in the generation of the eigenvectors from a training set of spectra are:

1. Noise-normalise each radiance spectrum and subtract the mean. Call the result  $y$ .
2. Form the covariance matrix from a large number ( $n$ ) of training spectra:

$$YY^T = (yy^T)$$

3. Generate the eigenvectors,  $U$ , using PCA:

$$YY^T / n = U\mathbf{w}U^T$$

AAPP then reads in the eigenvectors and computes the scores,  $c$ , for the near-real-time spectra,  $y$

$$c = U^T y'$$

The scores are stored in the IASI level 1d file.

AAPP update 6.6 includes a set of eigenvectors generated from 6 months of IASI data from July to December 2007. A set of 15736 spectra was used, generated by taking one day in every five, one 3-minute granule in every four, and between one and six spectra per granule depending on latitude – in order to avoid giving undue weight to polar spectra.

By default, AAPP de-apodises the spectra before computing the PC scores in order to ensure a diagonal noise covariance. But users can use apodised (level 1C) spectra if they prefer (e.g. time-critical applications).

Examination of the eigenvalues showed that the optimum number of PCs for the global training set is about 125-150: see Figure 1.

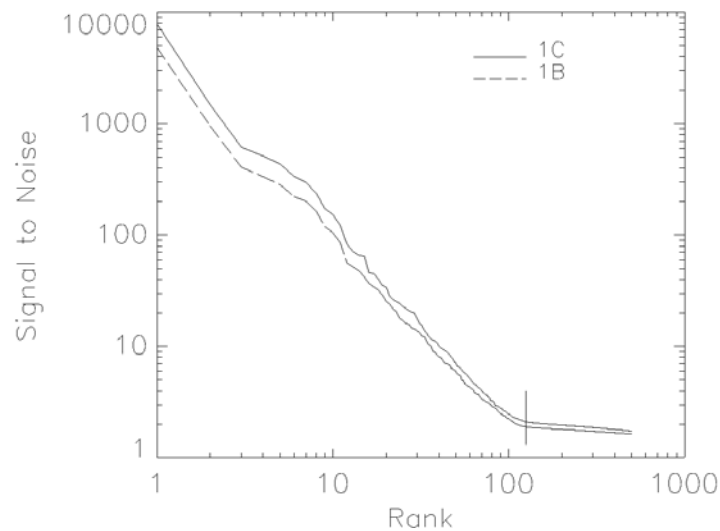


**Figure 1: Square root of the eigenvalues for training dataset.** The vertical line is at rank 125 and is where noise starts to dominate. The analysis has been carried out for both apodised spectra (1C) and de-apodised (1B), with similar results.

Since the instrument noise is roughly evenly distributed amongst the PCs, by retaining 150 PCs rather than all 8461 one would expect that the noise in the reconstructed radiances would be reduced by a factor  $\sqrt{(150/8461)} = 0.13$ . In practice this is probably rather optimistic, but simulations suggest that 0.18 should be achievable. For NWP this noise reduction would be expected to have the most impact for the stratospheric and upper tropospheric temperature sounding channels around  $650\text{-}750\text{ cm}^{-1}$ , where instrument noise is high relative to background error ( $\sim 0.3\text{K}$ ). The instrument noise, together with the AAPP default channel selection, is shown in Figure 2.

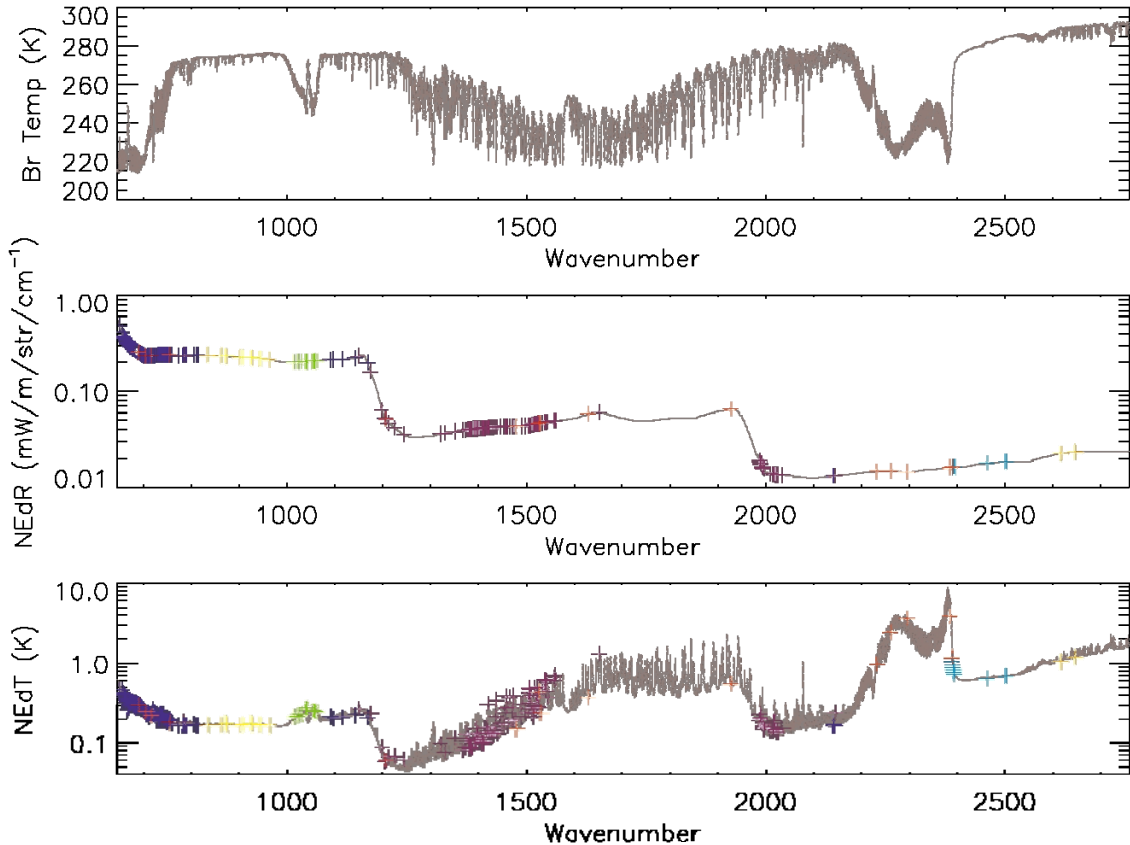


**Figure 2: IASI channel selection and noise characteristics.** Top: mean radiance spectrum from training set, converted to Brightness Temperature; Middle: Instrument random noise (1 $\sigma$ ) in radiance units; Bottom: Noise in Kelvin at the temperature corresponding to the mean radiance. The AAPP channel selection is shown by crosses. Colour key: **sounding**, **window**, **ozone**, **water vapour**, **solar**, **monitoring**.

### Regional ATOVS Retransmission Services

During 2007 and 2008 there has been a major expansion in the RARS networks. These networks are co-ordinated by WMO and aim to make ATOVS data available to users within 30 minutes of the observation. There are now three networks operating:

1. EARS-ATOVS, operated by EUMETSAT and covering parts of Europe, northern Atlantic, USA, Canada, Greenland and the Arctic. This service was established in 2002.
2. Asia Pacific RARS, with stations in Australia, Japan, China, Singapore, Korea and Antarctica.
3. South American RARS, with stations in Brazil, Argentina and Antarctica.

Each network comprises a number of HRPT reception stations, each running AAPP. The AMSU, MHS and HIRS level 1c files are then BUFR encoded and made available to users, typically via the GTS or EUMETCast. EUMETSAT also operate an AVHRR retransmission service, also based on AAPP.

In order to ensure global/local consistency, the NWP SAF monitors the incoming data and performs comparisons with the corresponding global data (typically received 2-3 hours later).

For further details on the NWP SAF monitoring activities, see

[http://www.metoffice.gov.uk/research/interproj/nwpsaf/ears\\_report/index.html](http://www.metoffice.gov.uk/research/interproj/nwpsaf/ears_report/index.html) .

Forecast impacts of using these more timely data have been shown to be positive (Candy, 2008), with potential for further improvement as new stations are established, especially in the southern hemisphere. For the current status of RARS, see <http://www.wmo.int/pages/prog/sat/RARS.html> .

## **NPP and NPOESS**

NPP is scheduled for launch in June 2010 and will contain a new suite of instruments, including CrIS, ATMS and VIIRS. It is planned to extend AAPP to accept data from these instruments – i.e. to develop 1d products for ATMS and CrIS that are analogous to the 1d products for AMSU/MHS and IASI.

AAPP will not process the direct broadcast data directly but the intention is that AAPP version 7 will be able to ingest the level 1 radiances generated by the *International Polar Orbiter Processing Package (IPOP)*, being prepared jointly by IPO, NASA and the University of Wisconsin (see <http://directreadout.gsfc.nasa.gov/index.cfm?section=technology&page=IPOP>). These data will be in HDF-5 format.

AAPP will also be able to ingest the BUFR format radiances that will be distributed through the NPOESS Data Exploitation (NDE) project. There is currently a proposal to redistribute VIIRS, ATMS and CrIS data to European users via EUMETCast.

A key requirement for NWP is that users have the flexibility to choose an appropriate effective spatial resolution for the ATMS 50GHz channels – which have a beam width of 2.2° and are sampled every 1.1° cross-track. For temperature sounding, users will often want to convert this data to an AMSU-A-like resolution (3.3° beam width), with low noise. On the other hand, for precipitation imaging there will be an interest in retaining the narrow beam width. Therefore AAPP will include beam width manipulation as an option, as well as the ability to map ATMS to CrIS.

In brief, the proposed technique is as follows:

1. With ATMS at its native spatial sampling, and treating each channel separately, perform a 2-D Fourier Transform (FT).
2. Multiply the transformed image by a pre-computed function that will broaden the effective beam shape. Gaussian beam shapes can be assumed when generating this function.
3. FT back to the image domain (still heavily over-sampled)
4. Interpolate to the CrIS sample positions if required, or re-sample at the required output grid.

Step 2 is illustrated in Figure 3. Note that we have attenuated high spatial frequencies, thereby reducing the noise; the RMS of the 2-dimensional ratio curve gives the noise reduction. The noise reduction factor is ~0.3 in the case illustrated – which should be sufficient to give AMSU-A-like noise levels for ATMS (~0.15K for the lower tropospheric temperature sounding channels). Some narrowing of the 23.8 and 31.4 GHz beam widths (from 5.2° to about 4.5°) will also be possible using this technique.

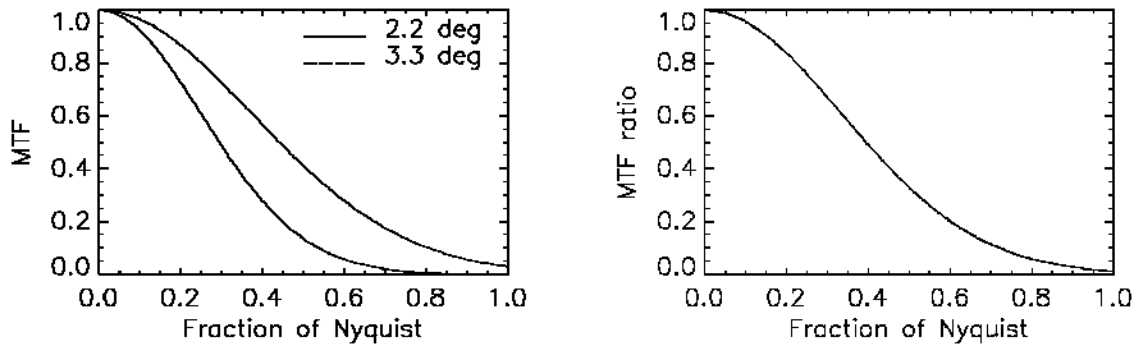


**Figure 3: Beam shape manipulation for ATMS.** Left: Spatial frequency response (Modulation Transfer Function, or MTF) for Gaussian beams of 2.2° and 3.3° beam width, sampled at 1.1°. Right: Ratio of the two response functions – to be used to multiply the FT of the input image. This is a 1-dimensional cross-section through a 2-D function.

The CrIS scan pattern is illustrated in Figure 4. AAPP will have the option of mapping ATMS to this scan pattern.

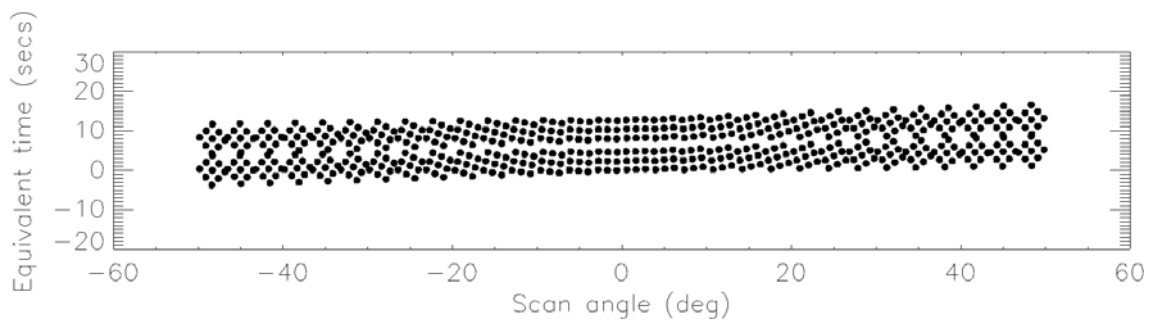


**Figure 4: Scan pattern for CrIS**

### Other developments

During 2008 and 2009, the following enhancements to AAPP version 6 are planned:

- Support for NOAA-N prime, scheduled for launch in February 2009
- A new version of the MAIA AVHRR cloud mask, supporting the AVHRR cluster analysis which forms part of the IASI level 1c dataset.

### Conclusions

AAPP version 6 is used operationally in many centres worldwide for processing direct-readout, regional and global data from the NOAA and MetOp satellites. FY-1D capability has recently been added.

AAPP is a key component of the RARS networks, which have undergone major expansions during 2007 and 2008. Global-local consistency is monitored by the NWP SAF.

The next AAPP major release (v7) will support NPP, due for launch in 2010.

## **Acknowledgements**

Thanks to the NWP SAF helpdesk team for their support in dealing with enquiries and distributing the software. Thanks also to AAPP users for their suggestions and feedback.

## **References**

- Atkinson, N.C., P. Brunel, P. Marguinaud and T. Labrot, 2006: AAPP status report and preparations for processing METOP data, *ITSC-15, Maratea, Italy, 4-10 October*, [http://cimss.ssec.wisc.edu/itwg/itsc/itsc15/proceedings/5\\_1\\_Atkinson.pdf](http://cimss.ssec.wisc.edu/itwg/itsc/itsc15/proceedings/5_1_Atkinson.pdf)
- Candy, B., 2008: Use of Regional Retransmission Networks in Global Data Assimilation, Poster A21, *ITSC-16, Angra dos Reis, Brazil, 7-13 May*
- Collard, A.D., 2007: Selection of IASI channels for use in numerical weather prediction, *ECMWF Technical Memorandum 532*, <http://www.ecmwf.int/publications/library/do/references/show?id=87881>
- Levin, V.A., A.I. Alexanin, M.G. Alexanina, D.A. Bolovin, A.V. Gromov and S.E. Diakov, 2005: Receiving and Processing of Chinese Meteorological Satellites FengYun Data in the Regional Centre of Far-Eastern Branch of Russian Academy of Sciences, *31st International Symposium on Remote Sensing of Environment, St. Petersburg, Russia, 20-24 May*, <http://www.isprs.org/publications/related/ISRSE/html/papers/611.pdf>
- Liu, Y., W. Zhang and Y. Zongdong, 1999: Fy-1c polar orbiting meteorological satellite of china: Satellite, ground system and preliminary applications, *Asian Conference on Remote Sensing, Hong Kong, China, 22-25 November*, <http://www.gisdevelopment.net/aars/acrs/1999/ps6/ps6211.asp>
- Marguinaud, P., P. Brunel and N.C. Atkinson, 2007: Validation of IASI OPS-LRS and comparison with global data, *First IASI conference, Anglet, France, 13-16 Nov*, <http://smc.cnes.fr/IASI/PDF/conf1/Brunel-poster.pdf>